Unmanned Systems, Vol. 14, No. 4 (2026) 853–886

DOI: 10.1142/S2301385026500238

UNMANNED SYSTEMS
https://www.worldscientific.com/worldscinet/us

Type-2 Fuzzy Adaptive Fault Tolerant Control Based on Disturbance Observer for Mobile Manipulator UAV Subject to External Disturbances and Parametric Uncertainties

Samir Zeghlache [*,§], Hilal Rahali [†,¶], Ali Djerioui [†,‖], Loutfi Benyettou [†,**], Mohamed Fouad Benkhoris [‡,††]

[*] *LASS, Laboratoire d'Analyse des Signaux et Systèmes, Department of Electrical Engineering, Faculty of Technology, University of M'sila University Pole, Road Bourdj Bou Arreiridj, M'sila 28000, Algeria*

[†] *LGE, Laboratoire de Génie Electrique, Department of Electrical Engineering, Faculty of Technology, University of M'sila University Pole, Road Bourdj Bou Arreiridj, M'sila 28000, Algeria*

[‡] *IREENA Laboratory, University of Nantes, Saint-Nazaire, France*

This work introduces a control approach for a mobile manipulator unmanned aerial vehicle (MMUAV) that is affected by numerous actuator defects, parametric uncertainties and external disturbances. The technique is based on a disturbance observer and adaptive type-2 fuzzy sliding mode control strategy. The suggested control method is unique among unmanned aerial vehicle (UAV) control strategies in that it can concurrently adjust for actuator defects, parametric uncertainties and external disturbances. The proposed control strategy utilizes adaptive control parameters in both continuous and discontinuous control components. This allows for the generation of suitable control signals to handle actuator faults and parametric uncertainties without entirely depending on the robust discontinuous control strategy of sliding mode control. Next, in order to preserve the tiny value of the discontinuous control gain of sliding mode control, a nonlinear disturbance observer is built and incorporated to reduce the impact of external disturbances. Furthermore, the stability study using Lyapunov's theory of the suggested control strategy demonstrates that it can maintain system tracking performance and minimize tracking errors in the given circumstances. Comparative simulation results of MMUAV under various failing and uncertain conditions show the efficiency of the suggested control approach.

Keywords: Type-2 fuzzy system; fault tolerant control; sliding mode control; adaptive control; unmanned aerial vehicle manipulator system.

1. Introduction

Unmanned aerial vehicles (UAVs) have been increasingly used in many sectors over the last several decades. These sectors include traffic surveillance [1, 2], conveyance of payloads [3, 4], agricultural precision [5], management, control and extinguishing wildfires [6], monitoring [7,8] and coordinated exploration [9]. So, a significant number of these uses are implemented in settings that need the highest levels of safety.

Furthermore, the increasing complexity of UAVs has prompted academics and manufacturers to focus more on their reliability and security [10]. Generally, UAVs are extensively used in hazardous and complicated situations at work, adding more dangers to their dependability and safety. The development of the last generation of UAVs necessitates the

Received 9 August 2024; Accepted 9 March 2025; Published 26 May 2025. This paper was recommended for publication in its revised form by editorial board member, Wei Meng.
Email Addresses: [§]samir.zeghlache@univ-msila.dz, [¶]hilal.rahali@univ-msila.dz, [‖]ali.djerioui@univ-msila.dz, [**]loutfi.benyettou@univ-msila.dz, [††]Mohamed-Fouad.Benkhoris@univ-nantes.fr
[§]Corresponding author.

integration of enhanced levels of autonomy and efficiency, as well as safety and security measures, in order to effectively fulfill their designated tasks. Quadrotor helicopters have received much attention among different kinds of UAVs, which is attributable to their ability to do vertical takeoff and landing (VTOL), their versatility of application for indoor and outdoor flight, and their low cost [11, 12].

In the future, UAVs are expected to be controlled using advanced algorithms that possess the capability to monitor the health state of UAVs and initiate appropriate measures as necessary [13, 14]. The growing need for superior system functionality, reliability and safety has led to extensive research on enhanced fault-tolerant control methods [15–17]. In [18], a comprehensive examination of fault-tolerant control and current fault diagnosis approaches for quadrotor UAVs is presented. There are active and passive fault-tolerant control methodologies in the world of quadrotor UAVs. There are two types of sliding modes in [19]: active and passive. These are based on fault-tolerant control techniques for tracking control in the event of an actuator defect. They are proposed and tested in a quadrotor UAV test bed, and their pros and cons are examined through theoretical and experimental research.

On the other hand, passive fault-tolerant control methods do not use fault information from an onboard fault diagnostic mechanism to change the controller to accommodate the fault. Active fault-tolerant control methods do. In [20], an active fault-tolerant control strategy based on a linear parameter-varying approach is used to counteract the bad effects of actuator faults. This scheme is used on an unmanned quadrotor helicopter. For a quadrotor UAV, the authors of [21] created two passive fault-tolerant controllers using the sliding mode concept in order to deal with partial actuator failures successfully. For passive fault-tolerant control techniques to work, they depend on how resilient the control strategy is to handle known faults. If faults do not happen, monitoring performance could be affected.

The authors of [22] developed a fault diagnostic unit that is capable of estimating actuator defects that result in ineffective control. This fault diagnosis unit is then integrated with a model reference adaptive control scheme to create an active fault-tolerant control system for a quadcopter system. Nevertheless, the degree of precision of the presented fault information has a significant impact on the performance of active fault-tolerant control techniques. Furthermore, it should be noted that the performance of the fault-tolerant control system may be affected by both the time delay and fault estimate error that are injected by the fault diagnostic unit [23]. Several researchers have focused their studies on adaptive fault-tolerant control approaches to address this issue [24]. It shows how a fault-tolerant monitoring control scheme can be used on a quadrotor UAV, along with an adaptive fault absorber, to reduce the effects of actuator failures. In [25], the authors develop an innovative adaptive fault-tolerant control system for a quadcopter attitude subsystem to maintain the required formation trajectory in the event of an actuator failure. The authors of [26] suggested a nonlinear adaptive fault-tolerant controller for a quadrotor UAV, which relies on an immersion and invariance observer, to address the issue of partial efficiency reduction caused by actuator malfunction. Model uncertainty and outside disturbances are problems that have yet to be fully studied, even though the control systems mentioned above can give quadrotor UAVs the performance they need for tracking even when actuators are broken.

Furthermore, the capacity for fault tolerance is one of many elements to consider while ensuring the dependability and security of UAVs. Indeed, practical systems often encounter several unpredictable aspects during their deployment for real applications [27–30]. One of the primary obstacles encountered in the operation of quadrotor UAVs is the management of outside perturbations and uncertainties in the model. For example, depending on the control applications, the variation and divergence in the placement and weight of the sensors and equipment installed on aircraft may be a substantial obstacle for aircraft control systems [31].

Several control approaches have been presented with the aim of improving the robustness of quadrotor controllers in the face of model uncertainty and outside perturbations. In [32], a composite control technique is developed to counteract the effects of time-varying perturbations on a quadrotor drone. In [33], a required performance controller is constructed using a backstepping approach to address the follow-up control issue of a quadrotor drone in the face of outside perturbations and uncertainties about the UAV's model. In [34], a second-order sliding mode controller is created for a quadrotor UAV with an imbalanced load to increase the resilience of the systems for flight control while taking into account complicated flying conditions. In [35], a sliding mode control method using backstepping and a cascade active perturbation rejection control is created to make sure that a quadrotor drone can track even when the UAV's model is uncertain and there are outside disturbances. In [36], this study proposes an anti-disturbance control strategy for a quadrotor UAV, which employs multiple observers to effectively minimize disturbances from both the wind and the cable-suspended payload. It should be noted that the above control techniques can only maintain strong tracking performance in the absence of faults. Because of this, to make sure the system is safe and reliable, the control system of a quadrotor UAV needs to be built so that it can handle actuator problems, outside disturbances and unknowns in the model system without affecting its functionality or putting its surroundings in danger. The system must efficiently tackle problems associated with actuator defects, external disturbances and alterations in parameters. In [37], a supplementary controller is devised to manage the concurrent appearance of two distinct categories of actuator defects. The control strategy that has been developed has a high level of robustness in the face of changing inertial parameters over time. It can also tolerate faults and achieve a high level of control precision. In [38], a resilient, defect-tolerant controller has been created to regulate the attitude of a quadrotor airplane in the presence of actuator defects and turbulent winds. In [39], a hybrid adaptive controller and backstepping approach based on type-2 fuzzy inference systems are presented. To compensate for these impacts, adjusted parameters are integrated into the suggested control. However, the majority of prior studies either consider all uncertain elements (such as actuator defects, uncertainties of model systems and outside perturbations) as a total perturbation or treat the uncertainties of model systems and outside perturbations as a single disturbance. When dealing with multiple simultaneous perturbations, this approach may result in a control method that is either conservative or completely ineffective. The predefined time fault-tolerant consensus tracking control issue has been formulated in [40] for UAV systems, including specified performance and attitude limitations. The UAV systems are categorized into position and attitude subsystems for analysis. A predefined-time consensus protocol is developed in the positioning subsystem by altering traditional prescribed performance control systems. The benefit of this work lies in its ability to maintain tracking errors that are continuously positive or negative during system operation while still achieving the required tracking accuracy within the specified. Inside the attitude subsystem, a universal barrier function based on output is created to enforce attitude output limits and get rid of the idea that Euler angles have to stay within certain ranges, which was a limitation in earlier research. Because UAV actuators can break down in harsh environments, an adaptive compensation technique is being developed to make multi-UAV systems more fault-tolerant. The work in [41] addressed the uncooperative target tracking control issue for UAVs underperformance and scaled relative velocity constraints, whereby the states of the uncooperative target may only be approximated via a vision sensor. Given the restricted detection range, a specified performance function is developed to guarantee both transient and steady-state performances of the tracking system.

The motivation of our research is to provide an effective fault reconstruction and tolerance strategy for the mobile manipulator unmanned aerial vehicle (MMUAV). Although tremendous research has been done to ensure the safe operation of quadrotor helicopters and to achieve precise tracking performance independent of model errors and external disturbances, there are still a few challenges that need to be solved.

(1) The vast majority of research on quadrotor helicopters has focused only on actuator defects or model uncertainties and disturbances in the published literature. Only a small number of studies, such as [42], have taken into account all of the potential unpredictability variables that might lead to a decline in control performance.
(2) The discontinuous control component is often overused to correct actuator problems using the sliding mode control approach. This may lead to control chattering, which in turn causes the system to fail to maintain its stability.
(3) Most observer-based control methods [43–45] treat unmodeled dynamics, changes in parameters and disturbances from the outside as a single type of disturbance that is evaluated by an observer. When there are many system disturbances, this approach may fail.

This paper presents a brand-new disturbance observer-based adaptive fault-tolerant control method that can handle actuator defects, parametric uncertainties and external disturbances simultaneously, making the system more resilient. UAV control systems should possess the capacity to withstand specific actuator failures, parametric uncertainties and external disturbances without jeopardizing themselves or their surroundings. From a control perspective, the objective is to develop a self-repairing "smart" flight control system to enhance the reliability and survivability of UAVs, as mandated by the next-generation flight control system outlined in the unmanned aircraft systems roadmap published in 2005 by the U.S. Department of Defense. This paper's main contributions are summarized as follows:

(1) Unlike the investigations in [46–48], the suggested control method has the potential to adaptively provide suitable control signals that can concurrently address actuator defects, parametric uncertainties and external disturbances instead of relying solely on the robust discontinuous control strategy of sliding mode control. When adaptive control parameters are used in both continuous and discontinuous control components, the discontinuous control component relies on much less, which makes control chattering less of a problem.
(2) The adaptive systems that have been put in place may prevent the adaptive control parameters from being overestimated, keeping the discontinuous control gain within a safe range. This is accomplished by using the boundary layer to formulate adaptive schemes instead of only relying on the sliding variable, as is common in most of the literature [49, 50].
(3) In contrast to the current fault-tolerant control methods for quadcopter systems developed in [51, 52], the design above approach combined the impact of actuator faults,

the uncertainties of model systems, and outside perturbations, leading to a conservative design approach. This paper addresses the issue of conservativeness by separately addressing and accommodating actuator faults, outside perturbations, and model uncertainties. In particular, the suggested adaptive type-2 fuzzy inference system schemes are used to account for model uncertainties and actuator failures. To account for changes in the outside world, a nonlinear disturbance observer is created.

(4) In [53, 54], passive fault-tolerant control based on nonlinear control has been proposed for hexacopter and quadrotor helicopters. This work presents a fault-tolerant control solution that integrates sliding mode control with adaptive interval-type-2 fuzzy inference systems improved by a nonlinear disturbance observer. Subsequently, it may address several categories of defects.

(6) Adaptive control is a method of control in which the controller adjusts to the controlled system, accommodating variations in parameters or addressing initial uncertainties. An adaptive controller for the octorotor and quadrotor helicopters has been developed, as referenced in [55–57]. This method demonstrated a rapid response that is not affected by external disturbances, eliminating the need for a precise model. System faults are not considered. This paper proposes an adaptive sliding mode control method using a type-2 fuzzy inference system and a nonlinear disturbance observer to address model uncertainties, external disturbances and actuator faults.

(7) An intelligent fuzzy controller has been extensively tested to control quadrotors in several works, such as [58, 59]. However, the trial-and-error problem severely limits these approaches. In [60], a type-2 fuzzy PID controller is designed to control the quadrotor helicopter, achieve trajectory tracking and reduce the influence of external disturbances, but it cannot deal with fault effects. In this paper, we propose an adaptive nonlinear control system that uses a disturbance observer to get position and angle control in a finite amount of time, even when there is uncertainty and an actuator fault.

Based on the observations above, different mechanisms are used to deal with actuator faults, parametric uncertainties and external disturbances. The proposed adaptive type-2 fuzzy inference system schemes handle actuator faults and parametric uncertainties, while a nonlinear disturbance observer reduces the effects of external disturbances. The developed disturbance observer also greatly reduces the size of the discontinuous control gain in sliding mode control, so it only needs to go above the threshold of the disturbance estimation error instead of the disturbance itself. This makes the control chattering problem a lot less severe.

This paper is arranged as follows. Modeling of MMUAV systems in defective conditions is presented in Sec. 2. In Sec. 3, conventional sliding mode control of the MMUAV system is synthesized. A background of the type-2 fuzzy logic inference system is then introduced in Sec. 4. The full design steps for the type-2 fuzzy adaptive sliding mode control synthesis and stability analysis are shown in Sec. 5. A disturbance observer design based on a type-2 fuzzy adaptive sliding mode control strategy is exposed in Sec. 6. The simulation results are presented and analyzed in Sec. 7. In Sec. 8, performances comparison with other approaches is performed. Finally, the conclusions of this paper are driven in Sec. 9.

2. Modeling of MMUAV System in Defective Condition

In order to examine actuator defects, multiplicative and additive models are used, as seen in Table 1 (refer to [61]).

t_f reflects the moment at which the actuator fails, whereas β indicates its coefficient of accuracy such that $\beta \in [-\bar{\beta}_0, \bar{\beta}_0]$, where $\bar{\beta}_0 > 0$. Also $\bar{k} \leq k \leq 1$, with $\bar{k} > 0$ denotes the minimal level of actuator capability, in which β and k are progressively varying, respectively, inside $[-\bar{\beta}_0, \bar{\beta}_0]$ and $[\bar{k}, 1]$ [61]. Table 1 illustrates many circumstances that might lead to actuator defeat in an MMUAV system. The dynamic model

Table 1. Actuator faults [61].

Actuators	Types of faults	Conditions	Names of faults
$U_i(t), i = 1, \dots, 4$	$U_i(t) + \beta_i(t)$	$\dot{\beta}_i(t) = 0, \beta_i(t_f) \neq 0$	Bias (lock in place)
	$\tau_j(t), j = 1, 2$	$\tau_j(t) + \vartheta_j(t)$	$\dot{\vartheta}_j(t) = 0, \vartheta_j(t_f) \neq 0$
	$U_i(t) + \beta_i(t)$	$\lvert\beta_i(t)\rvert = \xi_i t, 0 < \xi_i \ll 1$ for all $t \geq t_f$	Drift
	$\tau_j(t) + \vartheta_j(t)$	$\lvert\vartheta_j(t)\rvert = \alpha_j t, 0 < \alpha_j \ll 1$ for all $t \geq t_f$	
	$U_i(t) + \beta_i(t)$	$\lvert\beta_i(t)\rvert < \bar{\beta}_{0i}, \dot{\beta}_i(t) \to 0$ for all $t \geq t_f$	Loss of accuracy
	$\tau_j(t) + \vartheta_j(t)$	$\lvert\vartheta_j(t)\rvert < \bar{\vartheta}_{0j}, \dot{\vartheta}_j(t) \to 0$ for all $t \geq t_f$	
	$k_i(t)U_i(t)$	$0 < \bar{k}_i \leq k_i(t) \leq 1$ for all $t \geq t_f$	Loss of effectiveness
	$\Delta_j(t)\tau_j(t)$	$0 < \bar{\Delta}_j \leq \Delta_j(t) \leq 1$ for all $t \geq t_f$	

of the MMUAV is obtained in [62] by using Newton–Euler method expressed as

$$\begin{cases} \ddot{\varphi} = \left(\frac{I_{yy}-I_{zz}}{I_{xx}}\right)\dot{\theta}\dot{\psi} - \frac{U_{1f}(t)-\tau_r}{I_{xx}}, \\ \ddot{\theta} = \left(\frac{I_{zz}-I_{xx}}{I_{yy}}\right)\dot{\varphi}\dot{\psi} + \frac{g(m_1+m_2)C_z\sin(\theta)}{I_{xx}} \\ \quad - \frac{U_{2f}(t)-\tau_r}{I_{yy}}, \\ \ddot{\psi} = \left(\frac{I_{xx}-I_{yy}}{I_{zz}}\right)\dot{\varphi}\dot{\theta} - \frac{U_{3f}(t)}{I_{zz}}, \\ \ddot{z} = (c(\theta)c(\varphi))\frac{U_{4f}(t)}{m_T} - g, \\ \ddot{x} = (s(\psi)s(\varphi) + c(\psi)s(\theta)c(\varphi))\frac{U_{4f}(t)}{m_T}, \\ \ddot{y} = (s(\psi)s(\theta)c(\varphi) - c(\psi)s(\varphi))\frac{U_{4f}(t)}{m_T}, \\ \ddot{q} = M^{-1}(q)(\tau_f - C(q,\dot{q})\dot{q} - G(q) - F(\dot{q})), \end{cases} \tag{1}$$

where $\tau_f(t) = [\tau_{1f}(t)\ \tau_{2f}(t)]^T$.

To characterize the malfunctioning actuator for the difficulties mentioned in Table 1 [61], a short form may be used as follows:

$$U_{if}(t) = k_i(t)U_i(t) + \beta_i(t) \quad \text{for } i = 1,\dots,4, \tag{2}$$

$$\tau_{jf}(t) = \Delta_j(t)\tau_j(t) + \vartheta_j(t), \quad \text{for } j = 1,2. \tag{3}$$

By substituting (12) and (13) into (11), the MMUAV dynamic model's flawed condition is restructured in the following way:

$$\begin{cases} \ddot{\varphi} = \left(\frac{I_{yy}-I_{zz}}{I_{xx}}\right)\dot{\theta}\dot{\psi} - \frac{U_1(t)-\tau_r}{I_{xx}} + \Gamma_1(t) + d_1(t), \\ \ddot{\theta} = \left(\frac{I_{zz}-I_{xx}}{I_{yy}}\right)\dot{\varphi}\dot{\psi} + \frac{g(m_1+m_2)C_z s(\theta)}{I_{xx}} \\ \quad - \frac{U_2(t)-\tau_r}{I_{yy}} + \Gamma_2(t) + d_2(t), \\ \ddot{\psi} = \left(\frac{I_{xx}-I_{yy}}{I_{zz}}\right)\dot{\varphi}\dot{\theta} - \frac{U_3(t)}{I_{zz}} + \Gamma_3(t) + d_3(t), \\ \ddot{z} = (c(\theta)c(\varphi))\frac{U_4(t)}{m_T} - g + \Gamma_4(t) + d_4(t), \\ \ddot{x} = (s(\psi)s(\varphi) + c(\psi)s(\theta)c(\varphi))\frac{U_4(t)}{m_T} + \Gamma_5(t) + d_5(t), \\ \ddot{y} = (s(\psi)s(\theta)c(\varphi) - c(\psi)s(\varphi))\frac{U_4(t)}{m_T} + \Gamma_6(t) + d_6(t), \\ \ddot{q} = M^{-1}(q)(\tau(t) - C(q,\dot{q})\dot{q} - G(q) \\ \quad - F(\dot{q})) + \Gamma_7(t) + d_7(t), \end{cases} \tag{4}$$

where

$$\begin{aligned} \Gamma_1(t) &= \frac{-1}{I_{xx}}\{(k_1(t)-1)U_1(t) + \beta_1(t)\} \\ &\quad - \frac{1}{I_{xx}}\{\tau_1(t)(\sigma_1(t)-1) + \tau_2(t)(\sigma_2(t)-1) \\ &\quad + \vartheta_1(t) + \vartheta_2(t)\}, \\ \Gamma_2(t) &= \frac{-1}{I_{yy}}\{(k_2(t)-1)U_2(t) + \beta_2(t)\} - \frac{1}{I_{yy}} \\ &\quad \times \{\tau_1(t)(\sigma_1(t)-1) + \tau_2(t)(\sigma_2(t)-1) \\ &\quad + \vartheta_1(t) + \vartheta_2(t)\}, \\ \Gamma_3(t) &= \frac{-1}{I_{zz}}\{(k_3(t)-1)U_3(t) + \beta_3(t)\}, \\ \Gamma_4(t) &= \frac{(c(\theta)c(\varphi))}{m_T}\{(k_4(t)-1)U_4(t) + \beta_4(t)\}, \\ \Gamma_5(t) &= \frac{(s(\psi)s(\varphi) + c(\psi)s(\theta)c(\varphi))}{m_T} \\ &\quad \times \{(k_4(t)-1)U_4(t) + \beta_4(t)\}, \\ \Gamma_6(t) &= \frac{(s(\psi)s(\theta)c(\varphi) - c(\psi)s(\varphi))}{m_T} \\ &\quad \times \{(k_4(t)-1)U_4(t) + \beta_4(t)\}, \\ \Gamma_7(t) &= [(\sigma_1(t)-1)\tau_1(t) \\ &\quad + \vartheta_1(t)\ (\sigma_2(t)-1)\tau_2(t) + \vartheta_2(t)]^T. \end{aligned}$$

$\Gamma_1(t),\dots,\Gamma_7(t)$ describe the actuator faults effects.

$d_1(t),\dots,d_7(t)$ indicate external disturbances and uncertainties.

The roll angle, pitch angle and yaw angle are represented by the Euler angles φ, θ and ψ, respectively. x, y and z present the position of the origin of the body fixed-frame $\{o_i\}$ with respect to the inertial frame $\{o_v\}$ (Figs. 1 and 2), $q = [q_1\ q_2]^T$ indicates the angular position of the manipulator.

The MMUAV system's overall mass is denoted by m_T, with

$$m_T = m + m_1 + m_2, \tag{5}$$

where the hexacopter's mass is denoted by (m), (m_1) represents the mass of link 1, and (m_2) represents the mass of link 2.

The control inputs $(U_1(t), U_2(t), U_3(t), U_4(t))$ are provided as follows:

$$\begin{cases} U_1(t) = \frac{l\sqrt{3}}{2}(-F_2 - F_3 + F_5 + F_6), \\ U_2(t) = \frac{l}{2}(2F_1 + F_2 - F_3 - 2F_4 - F_5 + F_6), \\ U_3(t) = c_v(F_1 - F_2 + F_3 - F_4 + F_5 - F_6), \\ U_4(t) = F_1 + F_2 + F_3 + F_4 + F_5 + F_6, \end{cases} \tag{6}$$

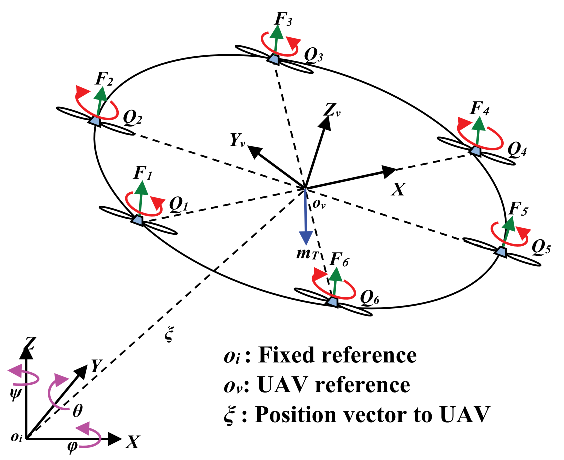

Fig. 1. Hexacopter configuration [62].

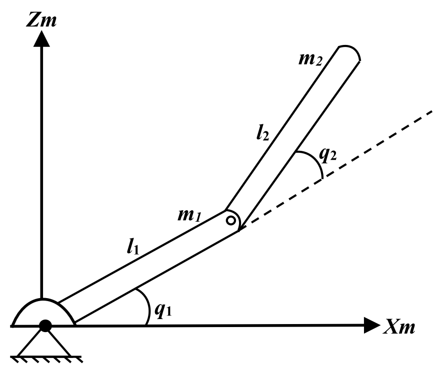

Fig. 2. Planar manipulator configuration [62].

where $(F_1, \dots, F_6)$ represents the forces generated by the six rotors, and c_v is the torque gain associated with the torque produces by six rotors. (I_{xx}, I_{yy}, I_{zz}) represents the MMUAV inertia moments, which are written as

$$\begin{cases} I_{xx} = I_x + \dfrac{m_1 l_1^2 s^3(q_1)}{3} + \dfrac{m_2 l_2^2 s^3(q_2)}{3} + m_2 l_1^2 s^2(q_1), \\ I_{yy} = I_y + \dfrac{m_1 l_1^2}{3} + \dfrac{m_2 l_2^2}{3} + m_2 l_1^2, \\ I_{zz} = I_z + \dfrac{m_1 l_1^2 c^3(q_1)}{3} + \dfrac{m_2 l_2^2 c^3(q_2)}{3} + m_2 l_1^2 c^2(q_1). \end{cases} \tag{7}$$

The hexacopter inertia moments are represented by I_x, I_y and I_z.

The manipulator's inertia matrix is given as

$$M(q) = \begin{bmatrix} M_{11} & M_{12} \\ M_{21} & M_{22} \end{bmatrix} \tag{8}$$

with

$$M_{11} = m_1 \left(\frac{l_1}{2}\right)^2 + m_2(l_1^2 + l_1 l_2(1 + c(q_2))) + I_1 + I_2,$$

$$M_{12} = M_{21} = m_2 \left(\frac{l_2}{2}\right)^2 + \left(\frac{l_1}{2}\right)\left(\frac{l_2}{2}\right)c(q_2)\Big) + I_2,$$

$$M_{22} = m_2 \left(\frac{l_2}{2}\right) + I_2.$$

I_1 and I_2 represent the inertia of each individual link in the manipulator.

The Coriolis matrix and the centrifugal forces exerted by the manipulator are expressed as

$$C(q, \dot{q}) = \begin{bmatrix} C_{11} & C_{12} \\ C_{21} & C_{22} \end{bmatrix}, \tag{9}$$

where

$$\begin{cases} C_{11} = -m_2 l_1 l_2 \dot{q}_2 s(q_2), \\ C_{12} = -m_2 l_1 l_2 (\dot{q}_1 + \dot{q}_2) s(q_2), \\ C_{21} = -m_2 l_1 l_2 \dot{q}_1 s(q_2), \\ C_{22} = 0. \end{cases}$$

The gravitational vector is given as follows:

$$G = [G_1 \quad G_2]^T \tag{10}$$

with

$$\begin{cases} G_1 = \left(m_1\left(\dfrac{l_1}{2}\right) + m_2 l_1\right) g c(q_1) + \left(m_2\left(\dfrac{l_2}{2}\right)\right) \\ \qquad \times c(q_1 + q_2), \\ G_2 = \left(m_2\left(\dfrac{l_2}{2}\right)\right) g c(q_1 + q_2). \end{cases}$$

The manipulator's control torque vector is denoted by $\tau(t) = [\tau_1(t)\ \tau_2(t)]^T$.

The friction forces vector is written as

$$F(\dot{q}) = 0.02[\text{sign}(\dot{q}_1)\ \text{sign}(\dot{q}_2)]^T, \tag{11}$$

where (τ_1, τ_2) stands the torque exerted by each link of the manipulator.

The expression of the torque τ_r generated by the manipulator which affects the hexacopter is given as

$$\tau_r = \tau_1 + m_2 g \left(\frac{l_1}{2}\right) c(q_1) + m_2 g \left(\frac{l_2}{2}\right) c(q_1 - q_2) + \tau_2. \tag{12}$$

The displacements of the centers of mass generated by the position of the manipulator are expressed as follows:

$$C_x = \frac{l_1 c(q_1)\left(\frac{m_1}{2} + m_2\right) + m_2 \frac{l_2}{2} c(q_1 - q_2)}{m_T}, \quad C_y = 0, \tag{13}$$

$$C_z = \frac{l_1 s(q_1)\left(\frac{m_1}{2} + m_2\right) + m_2 \frac{l_2}{2} s(q_1 - q_2)}{m_T}. \tag{14}$$

3. Conventional Sliding Mode Control of MMUAV System

The MMUAV mathematical model (14) may be expressed in state space form as follows:

$$\dot{X} = f(X, U(t), \tau(t)) + \Gamma(t) + D(t). \tag{15}$$

The state vector may be expressed as follows:

$$X = [x_1\ x_2\ x_3\ x_4\ x_5\ x_6\ x_7\ x_8\ x_9\ x_{10}\ x_{11}\ x_{12}\ x_{13}\ x_{14}]^T \in \Re^{14}, \tag{16}$$

where

$$\begin{cases} x_1 = \varphi, \quad x_4 = \dot{\theta}, \quad x_7 = z, \quad x_{10} = \dot{x}, \\ x_{13} = q, \quad x_2 = \dot{\varphi}, \quad x_5 = \psi, \quad x_8 = \dot{z}, \\ x_{11} = y, \quad x_{14} = \dot{q}, \quad x_3 = \theta, \\ x_6 = \dot{\psi}, \quad x_9 = x, \quad x_{12} = \dot{y}. \end{cases}$$

The input vectors are determined by

$$\begin{cases} U(t) = [U_1(t)\ U_2(t)\ U_3(t)\ U_4(t)]^T \in \Re^4, \\ \tau(t) = [\tau_1(t)\ \tau_2(t)]^T \in \Re^2. \end{cases} \tag{17}$$

The failures in actuators that affect the movement of the MMUAV have the following effects:

$$\Gamma(t) = [0\ \Gamma_1(t)\ 0\ \Gamma_2(t)\ 0\ \Gamma_3(t)\ 0\ \Gamma_4(t)\ 0\ \Gamma_5(t)\ 0\ \Gamma_6(t)\ 0 \Gamma_7(t)]^T \in \Re^{14}. \tag{18}$$

The external disturbances and uncertainties vector is given as

$$D(t) = [0\ d_1(t)\ 0\ d_2(t)\ 0\ d_3(t)\ 0\ d_4(t)\ 0\ d_5(t)\ 0\ d_6(t)\ 0\ d_7(t)]^T \in \Re^{14} \tag{19}$$

with

$$d_7(t) = \begin{bmatrix} d_{71}(t) \\ d_{72}(t) \end{bmatrix}.$$

The nonlinear function $f(X, U(t), \tau(t))$ is expressed as

$$f(X, U(t), \tau(t)) = \begin{pmatrix} x_2 \\ \left(\frac{I_{yy} - I_{zz}}{I_{xx}}\right) x_4 x_6 - \frac{U_1(t) - \tau_r}{I_{xx}} \\ x_4 \\ \left(\frac{I_{zz} - I_{xx}}{I_{yy}}\right) x_2 x_6 + \frac{g(m_1 + m_2) C_z \sin(x_3)}{I_{xx}} - \frac{U_2(t) - \tau_r}{I_{yy}} \\ x_6 \\ \left(\frac{I_{xx} - I_{yy}}{I_{zz}}\right) x_1 x_4 - \frac{U_3(t)}{I_{zz}} \\ x_8 \\ (\cos(x_1)\cos(x_3)) \frac{U_4(t)}{m_T} - g \\ x_{10} \\ (\sin(x_5)\sin(x_1) + \cos(x_5)\sin(x_3)\cos(x_1)) \frac{U_4(t)}{m_T} \\ x_{12} \\ (\sin(x_2)\sin(x_3)\cos(x_1) - \cos(x_5)\sin(x_1)) \frac{U_4(t)}{m_T} \\ x_{14} \\ M^{-1}(x_{13})(\tau(t) - C(x_{13}, x_{14}) x_{14} - G(x_{13}) - F(x_{14})) \end{pmatrix}.$$

3.1. *Virtual control*

The MMUAV's dynamic model consists of six different inputs $(U_1(t)\ U_2(t)\ U_3(t)\ U_4(t))$, $(\tau_1(t)\tau_2(t))$ and eight outputs $(\varphi\,\theta\,\psi\,z\,x\,y\,q_1\,q_2)$. Hence, the MMUAV may be classified as an underactuated system. It is not possible for us to exert control over all states at the same time [44]. Stable zero dynamics may be achieved in the system by combining controlled outputs $(\psi\,z\,x\,y\,q_1\,q_2)$ to track the desired positions and stabilize the roll and pitch angles $(\varphi\,\theta)$. In order to address this problem, it is necessary to include two more virtual control inputs $(U_5(t)\ U_6(t))$ into the existing six control inputs of the MMUAV. This will enable individual management of each output. The virtual control inputs $(U_5(t)\ U_6(t))$ represent the correlation between pitch-x movement and roll-y movement [45].

$$U_5(t) = (s(x_5)s(x_1) + c(x_5)s(x_3)c(x_1)), \tag{20}$$

$$U_6(t) = (s(x_2)s(x_3)c(x_1) - c(x_5)s(x_1)). \tag{21}$$

By using Eqs. (20) and (21), we obtain

$$\begin{cases} \varphi_d = \arcsin(U_5 s(x_5) - U_6 c(x_5)), \\ \theta_d = \arcsin\left(\frac{U_5 c(x_5) + U_6 s(x_5)}{c(\varphi_d)}\right). \end{cases} \tag{22}$$

The physical interpretation of virtual controls is that the roll and pitch angles determine the horizontal movement in the x and y directions. To achieve control over horizontal movement, the rolling and tilting movements should be adjusted to the appropriate angles $(\varphi_d\ \theta_d)$. Figure 3

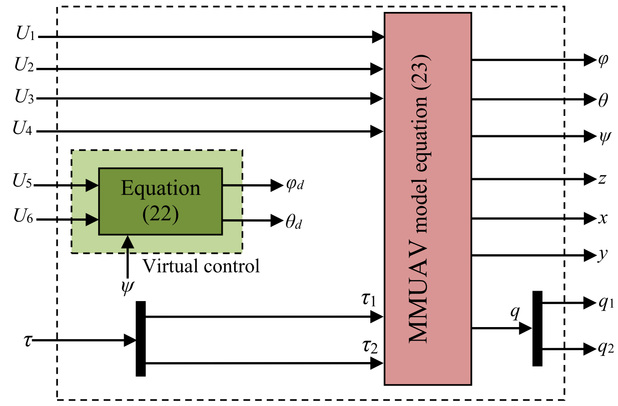

Fig. 3. Controlled the motion of an MMUAV utilizing virtual control.

displays the actuated MMUAV, which has eight inputs $(U_1(t)\ U_2(t)\ U_3(t)\ U_4(t)\ U_5(t)\ U_6(t))$ and $(\tau_1(t)\ \tau_2(t))$, as well as eight outputs $(\varphi\ \theta\ \psi\ z\ x\ y\ q_1\ q_2)$.

From the state space model (15), the subsequent configuration is feasible as follows:

$$\begin{cases} \dot{x}_{2n+1} = x_{2m}, \\ \dot{x}_{2m} = f_m(X) + g_m(X)U_m(t) + \delta_m(t), \\ \dot{x}_{13} = x_{14}, \\ \dot{x}_{14} = f_7(x_{13}, x_{14}) + M^{-1}(x_{13})\tau(t) + \delta_7(t), \end{cases} \tag{23}$$

where $n = 0, \ldots, 5$, $m = 1, \ldots, 6$, $f_m(X)$ and $f_7(x_{13}, x_{14})$ are unknown nonlinear functions defined as follows:

$$\begin{cases} f_1(X) = \left(\dfrac{I_{yy} - I_{zz}}{I_{xx}}\right) x_4 x_6 - \dfrac{\tau_r}{I_{xx}}, \quad g_1(X) = \dfrac{-1}{I_{xx}}, \\ f_2(X) = \left(\dfrac{I_{zz} - I_{xx}}{I_{yy}}\right) x_2 x_6 + \dfrac{g(m_1 + m_2)C_z s(x_3)}{I_{xx}} - \dfrac{\tau_r}{I_{yy}}, \\ g_2(X) = \dfrac{-1}{I_{yy}}, \quad f_3(X) = \left(\dfrac{I_{xx} - I_{yy}}{I_{zz}}\right) x_1 x_4, \\ g_3(X) = \dfrac{-1}{I_{zz}}, \quad f_4(X) = -g, \quad g_4(X) = \dfrac{c(x_1)c(x_3)}{m_T}, \\ f_5(X) = 0, \quad g_5(X) = \dfrac{U_4(t)}{m_T}, \\ f_6(X) = 0, \quad g_6(X) = \dfrac{U_4(t)}{m_T}, \\ f_7(x_{13}, x_{14}) = M^{-1}(x_{13})(-C(x_{13}, x_{14})x_{14} \\ \qquad - G(x_{13}) - F(x_{14})). \end{cases}$$

$$\begin{cases} \delta_m(t) = \Gamma_m(t) + d_m(t), \\ \delta_7(t) = \Gamma_7(t) + d_7(t). \end{cases} \tag{24}$$

The input vectors are specified as follows:

$$\begin{aligned} &U(t) = [U_1(t)\ U_2(t)\ U_3(t)\ U_4(t)\ U_5(t)\ U_6(t)]^T \in \Re^6, \\ &\tau(t) = [\tau_1(t)\ \tau_2(t)]^T \in \Re. \end{aligned} \tag{25}$$

The output vector is given as

$$Y = [\varphi\ \theta\ \psi\ z\ x\ y\ q_1\ q_2]^T \in \Re^8. \tag{26}$$

$\Gamma_m(t)$ and $\Gamma_7(t)$ represent the consequences of actuator defects, $d_m(t)$ and $d_7(t)$ are the effects of external disturbances and uncertainties.

The state space model in (23) can be rewritten as

$$\begin{cases} \dot{x}_{2n+1} = x_{2m}, \\ \dot{x}_{2m} = F_m(X) + g_m(X)U_m(t) + \alpha_m(t), \\ \dot{x}_{13} = x_{14}, \\ \dot{x}_{14} = F_7(x_{13}, x_{14}) + M^{-1}(x_{13})\tau(t) + \alpha_7(t), \end{cases} \tag{27}$$

where

$$\begin{aligned} F_m(X) &= f_m(X) + \Gamma_m(t), \\ \alpha_m(t) &= d_m(t), \\ F_7(x_{13}, x_{14}) &= f_7(x_{13}, x_{14}) + \Gamma_7(t), \\ \alpha_7(t) &= \begin{bmatrix} \alpha_{71}(t) \\ \alpha_{72}(t) \end{bmatrix} = d_7(t), \end{aligned}$$

$\alpha_m(t)$ and $\alpha_7(t)$ are components that group the external disturbances effects.

Assumption 1 ([31, 65]). The components that group the faults and external disturbances effects $\delta_m(t)$ and $\delta_7(t)$ in (23) are unknown but bounded and defined as $|\delta_m(t)| \leq D_{\alpha m}$ for $m = 1, \ldots, 6$ and $|\delta_7(t)| \leq D_{\alpha 7}$.

Sliding mode controllers are designed in two phases. A sliding surface must be built first to maintain system performance. Second, a control law is created to push the sliding variable to approach the desired surface and maintain its proximity.

For the reference signals $x_{(2n+1)d}$ and x_{13d}, we may establish the following definitions for the tracking error variables and their temporal derivatives:

$$\begin{cases} e_{2n+1} = x_{(2n+1)d} - x_{2n+1}, \quad n = 0, \ldots, 5, \\ e_{13} = x_{13d} - x_{13}, \end{cases} \tag{28}$$

$$\begin{cases} \dot{e}_{2n+1} = \dot{x}_{(2n+1)d} - x_{2m}, \quad n = 0, \ldots, 5, m = 1, \ldots, 6, \\ \dot{e}_{13} = \dot{x}_{13d} - x_{14}, \end{cases} \tag{29}$$

where $x_{13d} = q_d = [q_{1d}\ q_{2d}]^T$, $\dot{x}_{13d} = q_d = [\dot{q}_{1d}\ \dot{q}_{2d}]^T$, $x_{13} = q = [q_1\ q_2]^T$ and $x_{14} = \dot{q} = [\dot{q}_1\ \dot{q}_2]^T$.

The sliding surfaces can be defined as

$$s_{2n+1} = \dot{e}_{2n+1} + \lambda_{2n+1}(x_{(2n+1)d} - x_{2n+1}), \quad n = 0, \dots, 5, \tag{30}$$

$$s_{13} = \dot{e}_{13} + \lambda_{13}(x_{13d} - x_{13}) \tag{31}$$

with λ_{2n+1} and λ_{13} are positive design parameters.

Once the sliding surface has been designed, the next stage is to create a suitable control law that will enhance its attractiveness. The control law is structured as follows to meet this requirement:

$$\begin{cases} U_m(t) = U_{m,\mathrm{eq}}(t) + \Delta U_m, \\ \tau(t) = \tau_{\mathrm{eq}}(t) + \Delta\tau. \end{cases} \tag{32}$$

$U_{m,\mathrm{eq}}(t)$ and $\tau_{\mathrm{eq}}(t)$ represent the equivalent control components, whereas ΔU_m and $\Delta\tau$ represent the discontinuous control components used to achieve the intended sliding movement.

The equivalent control parts $U_{m,\mathrm{eq}}(t)$ and $\tau_{\mathrm{eq}}(t)$ are constructed by setting $\dot{s}_{2n+1} = 0$ and $\dot{s}_{13} = 0$, as shown in the following:

$$\begin{aligned} \dot{s}_{2n+1} &= \ddot{e}_{2n+1} + \lambda_{2n+1}(\dot{x}_{(2n+1)d} - \dot{x}_{2n+1}) \\ &= \ddot{x}_{(2n+1)d} + \lambda_{2n+1}(\dot{x}_{(2n+1)d} - \dot{x}_{2n+1}) - \dot{x}_{2m}, \\ &\qquad n = 0, 5 \text{ and } m = 1, \dots, 6, \end{aligned} \tag{33}$$

$$\begin{aligned} \dot{s}_{13} &= \ddot{e}_{13} + \lambda_{13}(\dot{x}_{13d} - \dot{x}_{13}) \\ &= \ddot{x}_{13d} + \lambda_{13}(\dot{x}_{13d} - \dot{x}_{13}) - \dot{x}_{14}. \end{aligned} \tag{34}$$

By replacing (23) into (33) and (34), the equivalent control inputs may be computed as follows:

$$\begin{cases} U_{m,\mathrm{eq}}(t) = \dfrac{1}{g_m(X)}(\ddot{x}_{(2n+1)d} + \lambda_{2n+1}(\dot{x}_{(2n+1)d} \\ \qquad - \dot{x}_{2n+1}) - f_m(X)), \\ \tau_{\mathrm{eq}}(t) = M(x_{13})\{\ddot{x}_{13d} + \lambda_{13}(\dot{x}_{13d} - \dot{x}_{13}) \\ \qquad - f_7(x_{13}, x_{14})\}. \end{cases} \tag{35}$$

Subsequently, a discontinuous control component is created to counteract disturbances and ensure the required sliding movement is maintained, while also keeping the sliding variable on the intended sliding surface. This control is synthesized as follows:

$$\begin{cases} \Delta U_m = \dfrac{1}{g_m(X)} k_{2n+1}\,\mathrm{sign}(s_{2n+1}), \\ \Delta\tau = M(x_{13}) k_{13}\,\mathrm{sign}(s_{13}), \end{cases} \tag{36}$$

where

$$k_{13} = \begin{bmatrix} k_{131} & 0 \\ 0 & k_{132} \end{bmatrix} = \mathrm{diag}\{k_{131}, k_{132}\}$$

and k_{2n+1} are positive design parameters.

The global control laws are formed by combining the equivalent and discontinuous control components as follows:

$$\begin{cases} U_m(t) = \dfrac{1}{g_m(X)}(\ddot{x}_{(2n+1)d} + \lambda_{2n+1}(\dot{x}_{(2n+1)d} \\ \qquad - \dot{x}_{2n+1}) - f_m(X) + k_{2n+1}\,\mathrm{sign}(s_{2n+1})), \\ \tau(t) = M(x_{13})\{\ddot{x}_{13d} + \lambda_{13}(\dot{x}_{13d} - \dot{x}_{13}) \\ \qquad - f_7(x_{13}, x_{14}) + k_{13}\,\mathrm{sign}(s_{13})\}. \end{cases} \tag{37}$$

Theorem 1. *Assume a nonlinear system in* (23), *with limited external disturbances. By using the global control laws in* (37) *and the designated sliding surfaces in* (30) *and* (31), *the intended sliding movement may be attained and sustained on the designated sliding surfaces, irrespective of disturbances. This is accomplished by selecting discontinuous control gains in* (36) *as* $k_{2n+1} \geq D_{\alpha m} + \eta_{2n+1}$ *for* $n = 0, 5$ *and* $m = 1, 6$ *and* $k_{13} = \mathrm{diag}\{k_{131}, k_{132}\} \geq \mathrm{diag}\{D_{\alpha 7} + \eta_{13}, D_{\alpha 7} + \eta_{13}\}$.

Proof. Define the following Lyapunov candidate functions as

$$V_{1,2n+1} = \frac{1}{2}s_{2n+1}^2, \quad n = 0, \dots, 5, \tag{38}$$

$$V_{1,13} = \frac{1}{2}s_{13}^T s_{13}. \tag{39}$$

The temporal derivatives of (38) and (39) are given as

$$\dot{V}_{1,2n+1} = s_{2n+1}\dot{s}_{2n+1}, \tag{40}$$

$$\dot{V}_{1,13} = s_{13}^T \dot{s}_{13}. \tag{41}$$

By replacing (33) into (40), we yield

$$\begin{aligned} \dot{V}_{1,2n+1} &= s_{2n+1}(\ddot{x}_{(2n+1)d} + \lambda_{2n+1}(\dot{x}_{(2n+1)d} - \dot{x}_{2n+1}) \\ &\quad - \ddot{x}_{(2n+1)d} - f_m(X) - \lambda_{2n+1}(\dot{x}_{(2n+1)d} \\ &\quad - \dot{x}_{2n+1}) + f_m(X) - k_{2n+1}\,\mathrm{sign}(s_{2n+1}) \\ &\quad - \alpha_m(t)), \quad m = 1, \dots, 6 \\ &= s_{2n+1}(-k_{2n+1}\,\mathrm{sign}(s_{2n+1}) - \alpha_m(t)) \\ &\leq (-[D_{\alpha m} + \eta_{2n+1}]|s_{2n+1}| - s_{2n+1}\alpha_m(t)) < 0. \end{aligned} \tag{42}$$

Replacing (34) into (41) leads to

$$\begin{aligned} \dot{V}_{1,13} &= s_{13}^T(\ddot{x}_{13d} + \lambda_{13}(\dot{x}_{13d} - \dot{x}_{13}) - M^{-1}(x_{13}) \\ &\quad \times (f_7(x_{13}, x_{14})) - \ddot{x}_{13d} - \lambda_{13}(\dot{x}_{13d} - \dot{x}_{13}) \\ &\quad + M^{-1}(x_{13})(f_7(x_{13}, x_{14})) - k_{13}\,\mathrm{sign}(s_{13}) - \alpha_7(t) \\ &= s_{13}^T(-k_{13}\,\mathrm{sign}(s_{13}) - \alpha_7(t)) \\ &= (-(k_{13}\,\mathrm{sign}(s_{13}))^T s_{13} - \alpha_7^T(t) s_{13}) \end{aligned}$$

$$\leq (-\text{diag}\{(D_{\alpha 7}+\eta_{13}),(D_{\alpha 7}+\eta_{13})\}|s_{13}| - \alpha_7^T(t)s_{13}) < 0. \tag{43}$$

Hence, by selecting small positive values of η_{2n+1} and η_{13}, the suggested global control laws in (37) ensure the stability of the system even in the face of faults and external disturbances.

Remark 1. Sliding mode control may mitigate fault and disturbance effects, but only if the discontinuous control gains k_{2n+1} and k_{13} are larger than the maximum disturbance. However, control chattering may occur if the discontinuous control gain is raised to ensure system stability as disturbances get stronger. In addition, the amount of chattering is directly proportional to the values of k_{2n+1} and k_{13}.

The implementation of the control laws in (44) is ineffective due to the need for a precise model. An adaptive control technique using type-2 fuzzy systems is offered as a solution to these kinds of issues. The proposed methodology is based on the use of online estimation to determine the local nonlinearities of each subsystem. These nonlinearities are represented by the functions $g_m(X)$, $f_m(X)$, $M_{ij}(x_{13})$ and $f_{7i}(x_{13},x_{14})$ for $m = 1,\dots,6$ and $(i,j) = 1,2$ are estimated using adaptive type-2 fuzzy systems and local state variables specific to each subsystem.

$$\begin{cases} U_m(t) = \dfrac{1}{g_m(X)}(\ddot{x}_{(2n+1)d} + \lambda_{2n+1}(\dot{x}_{(2n+1)d} \\ \qquad - \dot{x}_{2n+1}) - f_m(X) + k_{2n+1}\,\text{sign}(s_{2n+1})), \\ \tau(t) = \begin{bmatrix}\tau_1(t)\\ \tau_2(t)\end{bmatrix} = \begin{bmatrix} M_{11}(x_{13}) & M_{12}(x_{13}) \\ M_{12}(x_{13}) & M_{22}(x_{13})\end{bmatrix} \\ \qquad \times \Bigg\{\ddot{x}_{13d} + \lambda_{13}(\dot{x}_{13d} - \dot{x}_{13}) \\ \qquad - \begin{bmatrix} f_{71}(x_{13},x_{14}) \\ f_{72}(x_{13},x_{14})\end{bmatrix} + k_{13}\,\text{sign}(s_{13})\Bigg\}. \end{cases} \tag{44}$$

4. Background of the Type-2 Fuzzy Logic Inference System

Figure 4 illustrates the configuration of a type-2 fuzzy logic system. The system bears a resemblance to a type-1 fuzzy logic system. One important difference is that a type-2 fuzzy set is included, which means that a type reducer is needed to turn the fuzzy inference engine's output into a type-1 fuzzy set. This is called a type-reduced set. The set with reduced types is subjected to defuzzification in order to achieve a crisp result. In this study, we focus on the analysis of an interval-type-2 fuzzy logic system that employs singleton input fuzzification. The process of fuzzification is referred to as singleton fuzzification when the input fuzzy set consists of a single point with a degree of membership equal to 1. The use of interval type-2 fuzzy logic systems proves to be straightforward and efficient in streamlining the computing procedure for type reduction.

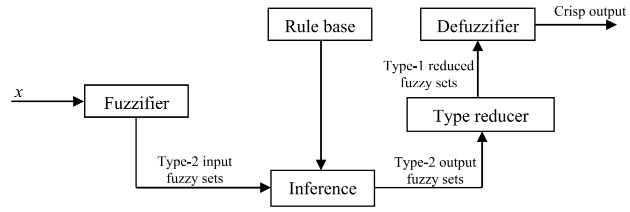

Fig. 4. Architecture of a type-2 fuzzy logic system.

Type-2 fuzzy logic controllers possess increased degrees of freedom and utilize fuzzy membership values, in contrast to type-1 fuzzy logic controllers, which employ crisp values. As a result, they provide a significant benefit by demonstrating greater resilience to elevated levels of uncertainty compared to type-1 fuzzy logic controllers. Type-2 fuzzy logic controllers demonstrate superior durability compared to type-1 fuzzy logic controllers, attributed to their capacity to manage a broader spectrum of operational environments.

Suppose we have a type-2 Takagi–Sugeno–Kang fuzzy logic system with n inputs, $x = [x_1,\dots,x_n] \in \Re^n$, and a single output, $y \in \Re$. In order to build the fuzzy rules, we suppose that the type-2 fuzzy system has N rules, where the Lth rule has the following form:

$$R^L : \text{if } x_1 \text{ is } \tilde{F}_1^L \quad \text{and } \dots \text{ and } x_n \text{ is } \tilde{F}_n^L \\ \text{then } y^L = C^L \quad L = 1,\dots,N. \tag{45}$$

The antecedent linguistic phrases, denoted as $\tilde{F}_1^L, \tilde{F}_2^L, \dots, \tilde{F}_n^L$, are represented by interval type-2 Gaussian fuzzy sets, as seen in Fig. 5. The output of the Lth rule R^L, is denoted as y^L, whereas the consequent parameter, C^L, is an interval type-1 set.

In Fig. 5, the uncertainty range of each membership function (MF) may be shown as a bounded interval using the

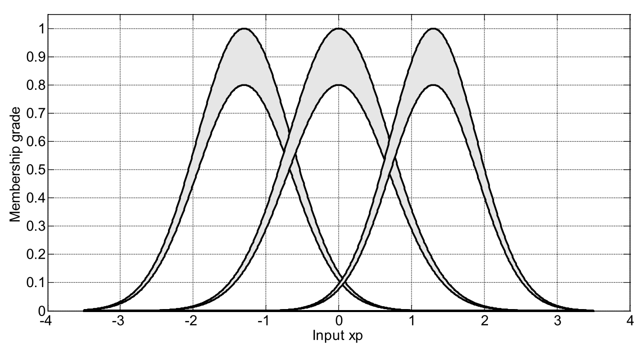

Fig. 5. Interval type-2 Gaussian membership functions for the antecedent sets.

upper MF $\bar{\mu}_{\tilde{F}_p^L}(x_p)$ and the lower MF $\underline{\mu}_{\tilde{F}_p^L}(x_p)$, where

$$\begin{cases} \bar{\mu}_{\tilde{F}_p^L}(x_p) = \exp\left\{-\frac{1}{2}\left(\frac{x_p - m_p}{\sigma_p}\right)^2\right\}, \\ \underline{\mu}_{\tilde{F}_p^L}(x_p) = 0.8\bar{\mu}_{\tilde{F}_p^L}(x_p). \end{cases} \tag{46}$$

In this context, σ_p and m_p represent respectively the mean and standard deviation of the Gaussian primary MF of the type-2 fuzzy system $\tilde{F}_p^L$ in the Lth rule.

The inference engine maps the crisp inputs to interval type-2 fuzzy output sets by combining the fuzzy rules. It takes the input and the rules' antecedents into account to determine the firing interval for each rule. Then, the subsequent fuzzy sets are trained using these firing levels. The Lth rule's firing interval, $[\underline{f}^L, \bar{f}^L]$, is a type-1 interval set that is defined by the points $\underline{f}^L$ and $\bar{f}^L$, which are located on the left and right sides of the set, respectively, such that

$$\underline{f}^L = \underline{\mu}_{\tilde{F}_1^L}(x_1) \times \underline{\mu}_{\tilde{F}_2^L}(x_2) \times \cdots \times \underline{\mu}_{\tilde{F}_n^L}(x_n) \tag{47}$$

$$\bar{f}^L = \bar{\mu}_{\tilde{F}_1^L}(x_1) \times \bar{\mu}_{\tilde{F}_2^L}(x_2) \times \cdots \times \bar{\mu}_{\tilde{F}_n^L}(x_n). \tag{48}$$

$\underline{\mu}_{\tilde{F}_p^L}(x_p)$ and $\bar{\mu}_{\tilde{F}_p^L}(x_p)$ denote the membership values of the lower and upper membership functions of the crisp input x_p to the type 2 fuzzy system $\tilde{F}_p^L$ in the Lth rule.

The final result may be stated as [66], when type-2 Takagi–Sugeno–Kang rules are applied with interval type-2 fuzzy systems for the antecedents and interval type-1 fuzzy systems for the consequent sets.

$$Y = [y_l y_r] = \int_{\theta^1} \cdots \int_{\theta^M} \cdots \int_{f^1} \cdots \int_{f^M} \times \frac{1}{\sum_{L=1}^N f^L \theta^L / \sum_{L=1}^N f^L}. \tag{49}$$

Considering that the output Y is a type-1 interval set, it is sufficient to calculate its two endpoints y_l and y_r using an expansion of fuzzy basis functions in the subsequent manner:

$$y_l = \frac{\sum_{L=1}^N f_l^L \theta^L}{\sum_{L=1}^N f_l^L} = \sum_{L=1}^N W_l^L(x)\theta^L = W_l^T(x)\theta, \tag{50}$$

$$y_r = \frac{\sum_{L=1}^N f_r^L \theta^L}{\sum_{L=1}^N f_r^L} = \sum_{L=1}^N W_r^L(x)\theta^L = W_r^T(x)\theta, \tag{51}$$

where f_l^L and f_r^L are the firing strength membership grades that contribute to y_l and y_r, respectively. Parameters θ^i represent type-1 centroids of consequent sets. Note that the centroid of a type-1 set C_L with Q discretized points is written as follows:

$$y_c = \frac{\sum_{L=1}^Q y_L \mu_{C^L}(y_L)}{\sum_{L=1}^Q \mu_{C^L}(y_L)}. \tag{52}$$

The fuzzy basis functions are obtained as

$$W_l^L(x) = \frac{f_l^L}{\sum_{L=1}^M f_l^L} \quad \text{and} \quad W_l^L(x) = \frac{f_r^L}{\sum_{L=1}^M f_r^L}. \tag{53}$$

Equation (53) denotes the components of the left and right fuzzy basis functions vectors are determined by

$$W_l^T(x) = [W_l^1(x), \dots, W_l^N(x)], \tag{54}$$

$$W_r^T(x) = [W_r^1(x), \dots, W_r^N(x)], \tag{55}$$

$$\theta = [\theta^1, \dots, \theta^N]. \tag{56}$$

To calculate y, it is necessary to calculate y_l and y_r. This may be accomplished by implementing the iterative algorithm provided in [67]. Here, a concise description of the computational process is given. First, we calculate the right-most point y_r.

For the sake of simplicity, let's suppose that the parameters θ_i are organized in ascending sequence, meaning that: $\theta^1 \le \theta^2 \le \cdots \theta^N$.

KM algorithm for y_r [67].

1. Calculate y_r in (51) by first assigning a starting value $f_r^L = \frac{\underline{f}^L + \bar{f}^L}{2}$ for $L = 1, 2, \dots, N$ with where $\underline{f}^L$ and $\bar{f}^L$ have been computed using (47) and (48), respectively, and let $y_r' = y_r$.
2. Determine the value of k (where $1 \le k \le N-1$) such that $\theta^k \le y_r' \le \theta^{k+1}$.
3. Calculate y_r in (17) where $f_r^L = \underline{f}^L$ for $L \le k$ and $f_l^L = \bar{f}^L$ for $L > k$; then, set $y_r'' = y_r$.
4. If $y_r'' \ne y_r'$, proceed to step 5. If $y_r'' = y_r'$, Establish thereafter $y_r = y_r''$, and proceed to step 6.
5. Set $y_r' = y_r''$, and proceed to step 2.
6. End

KM algorithm for y_l [67].

1. Calculate y_l in (50) by first assigning a starting value $f_l^L = \frac{\underline{f}^L + \bar{f}^L}{2}$ for $L = 1, 2, \dots, N$ with where $\underline{f}^L$ and $\bar{f}^L$ have been computed using (47) and (48), respectively, and let $y_l' = y_l$.
2. Determine the value of k' (where $1 \le k' \le N-1$) such that $\theta^{k'} \le y_l' \le \theta^{k'+1}$.
3. Calculate y_l in (17) where $f_l^L = \bar{f}^L$ for $L \le k'$ and $f_l^L = \underline{f}^L$ for $L > k'$; then, set $y_l'' = y_l$.
4. If $y_l'' \ne y_l'$, proceed to step 5. If $y_l'' = y_l'$, Establish thereafter $y_l = y_l''$, and proceed to step 6.
5. Set $y_l' = y_l''$, and proceed to step 2.
6. End

The average of y_l and y_r gives the type-2 fuzzy system's crisp output. Therefore, the defuzzified crisp output is obtained as

$$y = \frac{W_l^T(x) + W_r^T(x)}{2}\theta = W^T(x)\theta. \tag{57}$$

5. Type-2 Fuzzy Adaptive Sliding Mode Control Synthesis and Stability Analysis

Assumption 2 ([31, 65]). The disturbances effects $\alpha_m(t)$ and $\alpha_7(t)$ in (27) are unknown but bounded and defined as $|\alpha_m(t)| \le D_{\alpha m}$ for $m = 1, \dots, 6$ and $|\alpha_7(t)| \le D_{\alpha 7}$.

The suggested control technique utilizes four adaptive type-2 fuzzy inference system to approximate the functions $F_m(X_m)$, $g_m(X_m)$, $F_7(x_{13}, x_{14})$ and $M^{-1}(x_{13})$ separately. The approximation is done in the following manner:

$$F_m(X_m) = W_m^T(X_m)\theta_m^* + \varepsilon_{f_m} \quad \text{for } m = 1, \dots, 6, \tag{58}$$

$$g_m(X_m) = V_m^T(X_m)\vartheta_m^* + \varepsilon_{g_m} \quad \text{for } m = 1, \dots, 6, \tag{59}$$

$$F_7(x_{13}, x_{14}) = \begin{bmatrix} f_{71}(x_{13}, x_{14}) \\ f_{72}(x_{13}, x_{14}) \end{bmatrix} = \begin{bmatrix} W_{71}^T(x_{13}, x_{14})\theta_{71}^* + \varepsilon_{f_{71}} \\ W_{72}^T(x_{13}, x_{14})\theta_{72}^* + \varepsilon_{f_{72}} \end{bmatrix}, \tag{60}$$

$$F_7(x_{13}, x_{14}) = \begin{bmatrix} f_{71}(x_{13}, x_{14}) \\ f_{72}(x_{13}, x_{14}) \end{bmatrix} = \begin{bmatrix} W_{71}^T(x_{13}, x_{14})\theta_{71}^* + \varepsilon_{f_{71}} \\ W_{72}^T(x_{13}, x_{14})\theta_{72}^* + \varepsilon_{f_{72}} \end{bmatrix}, \tag{61}$$

where θ_m^*, ϑ_m^*, θ_{71}^*, θ_{72}^*, ϑ_{11}^*, ϑ_{12}^*, ϑ_{21}^* and ϑ_{22}^* are the ideal parameters, $W_m^T(X_m)$, $V_m^T(X_m)$, $W_{71}^T(x_{13}, x_{14})$, $W_{72}^T(x_{13}, x_{14})$, $V_{11}^T(x_{13})$, $V_{12}^T(x_{13})$, $V_{21}^T(x_{13})$ and $V_{22}^T(x_{13})$ are the mean basis functions obtained using type-2 fuzzy logic system. Each basis function is computed as the average of the respective left and right basis functions. The adaptive type-2 fuzzy inference system is considered to have limited approximation errors, denoted as

$$|\varepsilon_{f_m}| \le \varepsilon_{\alpha_{f_m}}, \quad |\varepsilon_{g_m}| \le \varepsilon_{\alpha_{g_m}}, \quad |\varepsilon_{f_{71}}| \le \varepsilon_{\alpha_{f_{71}}},$$
$$|\varepsilon_{f_{72}}| \le \varepsilon_{\alpha_{f_{72}}}, |\varepsilon_{M_{11}}| \le \varepsilon_{\alpha_{M_{11}}}, \quad |\varepsilon_{M_{12}}| \le \varepsilon_{\alpha_{M_{12}}},$$
$$|\varepsilon_{M_{21}}| \le \varepsilon_{\alpha_{M_{21}}} \quad \text{and} \quad |\varepsilon_{M_{22}}| \le \varepsilon_{\alpha_{M_{22}}}.$$

With $\varepsilon_{\alpha_{f_m}}, \varepsilon_{\alpha_{g_m}}, \varepsilon_{\alpha_{f_{71}}}, \varepsilon_{\alpha_{f_{72}}}, \varepsilon_{\alpha_{M_{11}}}, \varepsilon_{\alpha_{M_{12}}}, \varepsilon_{\alpha_{M_{21}}}$ and $\varepsilon_{\alpha_{M_{22}}}$ are unknown positive parameters.

The selected input vectors for the used type-2 fuzzy systems are determined as

$$\begin{cases} X_1 = [x_1 x_2]^T = [\varphi\dot{\varphi}]^T, \quad X_2 = [x_3 x_4]^T = [\theta\dot{\theta}]^T, \\ X_3 = [x_5 x_6]^T = [\psi\dot{\psi}]^T, \quad X_4 = [x_7 x_8]^T = [z\dot{z}]^T, \\ X_5 = [x_9 x_{10}]^T = [x\dot{x}]^T, \quad X_6 = [x_{11} x_{12}]^T = [y\dot{y}]^T, \\ x_{13} = [q_1 q_2]^T, \quad x_{14} = [\dot{q}_1 \dot{q}_2]^T. \end{cases} \tag{62}$$

The adaptive type-2 fuzzy inference system is primarily used to approximate the online nonlinear functions $F_m(X_m)$, $g_m(X_m)$, $F_7(x_{13}, x_{14})$ and $M^{-1}(x_{13})$. These functions are denoted as

$$\hat{F}_m(X_m) = W_m^T(X_m)\theta_m \quad \text{for } m = 1, \dots, 6, \tag{63}$$

$$\hat{g}_m(X_m) = V_m^T(X_m)\vartheta_m \quad \text{for } m = 1, \dots, 6, \tag{64}$$

$$\hat{F}_7(x_{13}, x_{14}) = \begin{bmatrix} \hat{f}_{71}(x_{13}, x_{14}) \\ \hat{f}_{72}(x_{13}, x_{14}) \end{bmatrix} = \begin{bmatrix} W_{71}^T(x_{13}, x_{14})\theta_{71} \\ W_{72}^T(x_{13}, x_{14})\theta_{72} \end{bmatrix}, \tag{65}$$

$$\hat{M}^{-1}(x_{13}) = \begin{bmatrix} \hat{M}_{11}(x_{13}) & \hat{M}_{12}(x_{13}) \\ \hat{M}_{12}(x_{13}) & \hat{M}_{22}(x_{13}) \end{bmatrix} = \begin{bmatrix} V_{11}^T(x_{13})\vartheta_{11} & V_{12}^T(x_{13})\vartheta_{12} \\ V_{12}^T(x_{13})\vartheta_{12} & V_{22}^T(x_{13})\vartheta_{22} \end{bmatrix}, \tag{66}$$

where θ_m, ϑ_m, θ_{71}, θ_{72}, ϑ_{11}, ϑ_{12}, ϑ_{21} and ϑ_{22} are the adjusted vector parameters.

By using Eqs. (57)–(60) and (62)–(65), it can be shown that

$$\begin{cases} \hat{F}_m(X_m) - F_m(X_m) = -W_m^T(X_m)\tilde{\theta}_m - \varepsilon_{f_m}, \\ \hat{g}_m(X_m) - g_m(X_m) = -V_m^T(X_m)\tilde{\vartheta}_m - \varepsilon_{g_m}, \end{cases} \tag{67}$$

$$\hat{F}_7(x_{13}, x_{14}) - F_7(x_{13}, x_{14}) = \begin{bmatrix} \hat{F}_{71}(x_{13}, x_{14}) \\ \hat{F}_{72}(x_{13}, x_{14}) \end{bmatrix} - \begin{bmatrix} F_{71}(x_{13}, x_{14}) \\ F_{72}(x_{13}, x_{14}) \end{bmatrix} = \begin{bmatrix} -W_{71}^T(x_{13}, x_{14})\tilde{\theta}_{71} - \varepsilon_{f_{71}} \\ -W_{72}^T(x_{13}, x_{14})\tilde{\theta}_{72} - \varepsilon_{f_{72}} \end{bmatrix}. \tag{68}$$

$$\begin{aligned} \hat{M}^{-1}(x_{13}) - M^{-1}(x_{13}) &= \begin{bmatrix} \hat{M}_{11}(x_{13}) & \hat{M}_{12}(x_{13}) \\ \hat{M}_{12}(x_{13}) & \hat{M}_{22}(x_{13}) \end{bmatrix} - \begin{bmatrix} M_{11}(x_{13}) & M_{12}(x_{13}) \\ M_{12}(x_{13}) & M_{22}(x_{13}) \end{bmatrix}, \\ &= \begin{bmatrix} -V_{11}^T(x_{13})\tilde{\vartheta}_{11} - \varepsilon_{M_{11}} & -V_{12}^T(x_{13})\tilde{\vartheta}_{12} - \varepsilon_{M_{12}} \\ -V_{12}^T(x_{13})\tilde{\vartheta}_{12} - \varepsilon_{M_{12}} & -V_{22}^T(x_{13})\tilde{\vartheta}_{22} - \varepsilon_{M_{22}} \end{bmatrix}, \end{aligned} \tag{69}$$

where $\tilde{\theta}_m = \theta_m^* - \theta_m$, $\tilde{\vartheta}_m = \vartheta_m^* - \vartheta_m$, $\tilde{\theta}_{71} = \theta_{71}^* - \theta_{71}$, $\tilde{\theta}_{72} = \theta_{72}^* - \theta_{72}$, $\tilde{\vartheta}_{11} = \vartheta_{11}^* - \vartheta_{11}$, $\tilde{\vartheta}_{12} = \vartheta_{12}^* - \vartheta_{12}$, $\tilde{\vartheta}_{21} = \vartheta_{21}^* - \vartheta_{21}$ and $\tilde{\vartheta}_{22} = \vartheta_{22}^* - \vartheta_{22}$ are the parametric errors.

The feedback control law is ultimately formulated as

$$\begin{cases} U_m(t) = \dfrac{1}{\hat{g}_m(X)}(\ddot{x}_{(2n+1)d} + \lambda_{2n+1}(\dot{x}_{(2n+1)d} \\ \quad - \dot{x}_{2n+1}) - \hat{F}_m(X)) + \dfrac{1}{\hat{g}_m(X)} \\ \quad \times k_{2n+1}\,\mathrm{sign}(s_{2n+1}), \\ \tau(t) = \begin{bmatrix}\tau_1(t)\\ \tau_2(t)\end{bmatrix} \\ \quad = \hat{M}(x_{13})\{\ddot{x}_{13d} + \lambda_{13}(\dot{x}_{13d} - \dot{x}_{13}) \\ \quad - \hat{F}_7(x_{13}, x_{14})\} + \hat{M}(x_{13})k_{13}\,\mathrm{sign}(s_{13}). \end{cases} \tag{70}$$

The following rules define the adjustment of type-2 fuzzy system parameters:

$$\begin{cases} \dot{\theta}_m = -a_{1m}s_{2n+1}W_m(X_m), \\ \dot{\vartheta}_m = -a_{2m}s_{2n+1}V_m(X_m)U_m(t), \\ \dot{\theta}_{71} = -a_{71}B_1 s_{13}W_{71}(x_{13}, x_{14}), \\ \dot{\theta}_{72} = -a_{72}B_2 s_{13}W_{72}(x_{13}, x_{14}), \\ \dot{\vartheta}_{11} = -A_{11}B_1 s_{13}V_{11}(x_{13})\tau_1(t), \\ \dot{\vartheta}_{12} = -A_{12}B_1 s_{13}V_{12}(x_{13})\tau_2(t), \\ \dot{\vartheta}_{21} = -A_{21}B_2 s_{13}V_{21}(x_{13})\tau_1(t), \\ \dot{\vartheta}_{22} = -A_{22}B_2 s_{13}V_{22}(x_{13})\tau_2(t) \end{cases} \tag{71}$$

with $B_1 = [1\ 0]$, $B_2 = [0\ 1]$ and a_{1m}, a_{2m}, a_{71}, a_{72}, A_{11}, A_{12}, A_{21} and A_{22} are positive tuning parameters.

Remark 2. (1) The control law in (44) is only true over a compact set $U_c \subset R^n$ on which $g_m(X) > 0$.

(2) The developed control law in (70) incorporates the adaptive control parameters $\frac{1}{\hat{g}_m(X)}$ and $\hat{M}(x_{13})$ which are utilized in both the continuous and discontinuous control components. Following the occurrence of an actuator fault, the continuous control component will assist in fault accommodation, thereby minimizing the reliance on the discontinuous part of sliding mode control. The proposed control scheme effectively mitigates the control chattering problem.

(3) In the implementation of the adaptive controller, the condition $\hat{g}_m(X) > 0$ should be guaranteed, because the proposed controller (70) has the inverse term of $\hat{g}_m(X)$. Therefore, we choose the initial type-2 fuzzy system parameters vector values (i.e., $\vartheta_m(0)$) are small positive constants in simulations.

Theorem 2. *Let's assume a nonlinear system in Eq.* (27) *that incorporates both actuator defects and external disturbances. Using the control laws in* (70) *and adding the suggested adaptation laws in* (71), *the desired sliding movement can be made and kept up, even if there are problems with the actuators or disturbances from the outside. The discontinuous control gains are represented as follows*:

$$k_{13} = \mathrm{diag}\{k_{131}, k_{132}\} \geq [\mathrm{diag}\{(D_{\alpha 7} + \eta_{13}), (D_{\alpha 7} \\ + \eta_{13})\}] + [\mathrm{diag}\{|\varepsilon_{f_{71}} + \varepsilon_{M_{11}}\tau_1(t) + \varepsilon_{M_{12}}\tau_2(t)|, \\ \times |\varepsilon_{f_{72}} + \varepsilon_{M_{21}}\tau_1(t) + \varepsilon_{M_{22}}\tau_2(t)|\}]$$

and $k_{2n+1} \geq D_{\alpha m} + |\varepsilon_{f_m} + \varepsilon_{g_m}U_m(t)| + \eta_{2n+1}$ *are chosen for this purpose.*

Proof. Define the following Lyapunov candidate functions as

$$V_{2,2n+1} = \frac{1}{2}s_{2n+1}^2 + \frac{1}{a_{1m}}\tilde{\theta}_m^T\tilde{\theta}_m \\ + \frac{1}{a_{2m}}\tilde{\vartheta}_m^T\tilde{\vartheta}_m, \quad n = 0, \ldots, 5\ m = 1, \ldots, 6, \tag{72}$$

$$V_{2,13} = \frac{1}{2}s_{13}^T s_{13} + \frac{1}{a_{71}}\tilde{\theta}_{71}^T\tilde{\theta}_{71} + \frac{1}{a_{72}}\tilde{\theta}_{72}^T\tilde{\theta}_{72} \\ + \frac{1}{a_{11}}\tilde{\vartheta}_{11}^T\tilde{\vartheta}_{11} + \frac{1}{a_{12}}\tilde{\vartheta}_{12}^T\tilde{\vartheta}_{12} + \frac{1}{a_{21}}\tilde{\vartheta}_{21}^T\tilde{\vartheta}_{21} \\ + \frac{1}{a_{22}}\tilde{\vartheta}_{22}^T\tilde{\vartheta}_{22}. \tag{73}$$

The temporal derivative of the sliding surfaces in (30) and (31) may be calculated as follows:

$$\dot{s}_{2n+1} = \ddot{x}_{(2n+1)d} + \lambda_{2n+1}(\dot{x}_{(2n+1)d} - \dot{x}_{2n+1}) - F_m(X) \\ - g_m(X)U_m(t) - \alpha_m(t) \tag{74}$$

$$\dot{s}_{13} = \ddot{x}_{13d} + \lambda_{13}(\dot{x}_{13d} - \dot{x}_{13}) - F_7(x_{13}, x_{14}) \\ - M^{-1}(x_{13})\tau(t) - \alpha_7(t). \tag{75}$$

By adding and subtracting the terms $\hat{g}_m(X)U_m(t)$ in (74), we get the following:

$$\dot{s}_{2n+1} = \ddot{x}_{(2n+1)d} + \lambda_{2n+1}(\dot{x}_{(2n+1)d} - \dot{x}_{2n+1}) - F_m(X) \\ - \hat{g}_m(X)U_m(t) + \{\hat{g}_m(X) - g_m(X)\}U_m(t) \\ - \alpha_m(t). \tag{76}$$

By adding and subtracting the terms $\hat{M}^{-1}(x_{13})\tau(t)$ in (75), we get the following:

$$\dot{s}_{13} = \ddot{x}_{13d} + \lambda_{13}(\dot{x}_{13d} - \dot{x}_{13}) - F_7(x_{13}, x_{14}) \\ - \hat{M}^{-1}(x_{13})\tau(t) + \{\hat{M}^{-1}(x_{13}) - M^{-1}(x_{13})\}\tau(t) \\ - \alpha_7(t). \tag{77}$$

By replacing the control laws $U_m(t)$, $\tau(t)$ in (70) into (76) and (77)

$$\dot{s}_{2n+1} = \ddot{x}_{(2n+1)d} + \lambda_{2n+1}(\dot{x}_{(2n+1)d} - \dot{x}_{2n+1}) \\ - F_m(X) - (\ddot{x}_{(2n+1)d} + \lambda_{2n+1}(\dot{x}_{(2n+1)d}$$

$$- \dot{x}_{2n+1}) - \hat{F}_m(X) + k_{2n+1} \operatorname{sign}(s_{2n+1}))$$
$$+ \{\hat{g}_m(X) - g_m(X)\}U_m(t) - \alpha_m(t)$$
$$= [\hat{F}_m(X) - F_m(X)] - k_{2n+1} \operatorname{sign}(s_{2n+1})$$
$$+ \{\hat{g}_m(X) - g_m(X)\}U_m(t) - \alpha_m(t), \tag{78}$$

$$\begin{aligned}\dot{s}_{13} &= \ddot{x}_{13d} + \lambda_{13}(\dot{x}_{13d} - \dot{x}_{13}) - F_7(x_{13}, x_{14}) \\ &\quad - (\ddot{x}_{13d} + \lambda_{13}(\dot{x}_{13d} - \dot{x}_{13}) - \hat{F}_7(x_{13}, x_{14}) \\ &\quad + k_{13} \operatorname{sign}(s_{13})) + \{\hat{M}^{-1}(x_{13}) - M^{-1}(x_{13})\} \\ &\quad \times \tau(t) - \alpha_7(t) \\ &= [\hat{F}_7(x_{13}, x_{14}) - F_7(x_{13}, x_{14})] - k_{13} \operatorname{sign}(s_{13}) \\ &\quad + \{\hat{M}^{-1}(x_{13}) - M^{-1}(x_{13})\}\tau(t) - \alpha_7(t). \end{aligned} \tag{79}$$

By substituting (66), (67) into (78) and (68), (69) into (79), yields:

$$\begin{aligned}\dot{s}_{2n+1} &= [-W_m^T(X_m)\tilde{\theta}_m - \varepsilon_{f_m}] - k_{2n+1} \operatorname{sign}(s_{2n+1}) \\ &\quad + \{-V_m^T(X_m)\tilde{\vartheta}_m - \varepsilon_{g_m}\}U_m(t) - \alpha_m(t), \end{aligned} \tag{80}$$

$$\begin{aligned}\dot{s}_{13} &= \begin{bmatrix} -W_{71}^T(x_{13}, x_{14})\tilde{\theta}_{71} - \varepsilon_{f_{71}} \\ -W_{72}^T(x_{13}, x_{14})\tilde{\theta}_{72} - \varepsilon_{f_{72}} \end{bmatrix} - k_{13} \operatorname{sign}(s_{13}) \\ &\quad + \begin{bmatrix} -V_{11}^T(x_{13})\tilde{\vartheta}_{11} - \varepsilon_{M_{11}} & -V_{12}^T(x_{13})\tilde{\vartheta}_{12} - \varepsilon_{M_{12}} \\ -V_{21}^T(x_{13})\tilde{\vartheta}_{21} - \varepsilon_{M_{21}} & -V_{22}^T(x_{13})\tilde{\vartheta}_{22} - \varepsilon_{M_{22}} \end{bmatrix} \\ &\quad \times \tau(t) - \alpha_7(t). \end{aligned} \tag{81}$$

Then, the temporal derivative of the chosen Lyapunov candidate functions in (72) and (73) can be expressed as

$$\dot{V}_{2,2n+1} = s_{2n+1}\dot{s}_{2n+1} + \frac{1}{a_{1m}}\tilde{\theta}_m^T\dot{\tilde{\theta}}_m + \frac{1}{a_{2m}}\tilde{\vartheta}_m^T\dot{\tilde{\vartheta}}_m, \tag{82}$$

$$\begin{aligned}\dot{V}_{2,13} &= s_{13}^T\dot{s}_{13} + \frac{1}{a_{71}}\tilde{\theta}_{71}^T\dot{\tilde{\theta}}_{71} + \frac{1}{a_{72}}\tilde{\theta}_{72}^T\dot{\tilde{\theta}}_{72} \\ &\quad + \frac{1}{a_{11}}\tilde{\vartheta}_{11}^T\dot{\tilde{\vartheta}}_{11} + \frac{1}{a_{12}}\tilde{\vartheta}_{12}^T\dot{\tilde{\vartheta}}_{12} + \frac{1}{a_{21}}\tilde{\vartheta}_{21}^T\dot{\tilde{\vartheta}}_{21} \\ &\quad + \frac{1}{a_{22}}\tilde{\vartheta}_{22}^T\dot{\tilde{\vartheta}}_{22}. \end{aligned} \tag{83}$$

By substituting (80) into (82) and (81) into (83), we get

$$\begin{aligned}\dot{V}_{2,2n+1} &= s_{2n+1}([-W_m^T(X_m)\tilde{\theta}_m - \varepsilon_{f_m}] - k_{2n+1} \\ &\quad \times \operatorname{sign}(s_{2n+1}) + \{-V_m^T(X_m)\tilde{\vartheta}_m - \varepsilon_{g_m}\} \\ &\quad \times U_m(t) - \alpha_m(t)) - \frac{1}{a_{1m}}\tilde{\theta}_m^T\dot{\theta}_m - \frac{1}{a_{2m}}\tilde{\vartheta}_m^T\dot{\vartheta}_m \\ &= \tilde{\theta}_m^T\left(-s_{2n+1}W_m(X_m) - \frac{1}{a_{1m}}\dot{\theta}_m\right) + \tilde{\vartheta}_m^T \\ &\quad \times \left(-s_{2n+1}V_m(X_m)U_m(t) - \frac{1}{a_{2m}}\dot{\vartheta}_m\right) \\ &\quad + s_{2n+1}(-\varepsilon_{f_m} - k_{2n+1} \operatorname{sign}(s_{2n+1}) \\ &\quad - \varepsilon_{g_m}U_m(t) - \alpha_m(t)) \end{aligned} \tag{84}$$

$$\begin{aligned}\dot{V}_{2,13} &= s_{13}^T\left[\begin{bmatrix} -W_{71}^T(x_{13}, x_{14})\tilde{\theta}_{71} - \varepsilon_{f_{71}} \\ -W_{72}^T(x_{13}, x_{14})\tilde{\theta}_{72} - \varepsilon_{f_{72}} \end{bmatrix} - k_{13} \operatorname{sign}(s_{13}) \right. \\ &\quad + \begin{bmatrix} -V_{11}^T(x_{13})\tilde{\vartheta}_{11} - \varepsilon_{M_{11}} & -V_{12}^T(x_{13})\tilde{\vartheta}_{12} - \varepsilon_{M_{12}} \\ -V_{21}^T(x_{13})\tilde{\vartheta}_{21} - \varepsilon_{M_{21}} & -V_{22}^T(x_{13})\tilde{\vartheta}_{22} - \varepsilon_{M_{22}} \end{bmatrix}\tau(t) - \alpha_7(t) \Bigg] \\ &\quad - \frac{1}{a_{71}}\tilde{\theta}_{71}^T\dot{\theta}_{71} - \frac{1}{a_{72}}\tilde{\theta}_{72}^T\dot{\theta}_{72} - \frac{1}{a_{11}}\tilde{\vartheta}_{11}^T\dot{\vartheta}_{11} \\ &\quad - \frac{1}{a_{12}}\tilde{\vartheta}_{12}^T\dot{\vartheta}_{12} - \frac{1}{a_{21}}\tilde{\vartheta}_{21}^T\dot{\vartheta}_{21} - \frac{1}{a_{22}}\tilde{\vartheta}_{22}^T\dot{\vartheta}_{22} \\ &= -s_{13}^T\begin{bmatrix} \tilde{\theta}_{71}^T & 0 \\ 0 & \tilde{\theta}_{72}^T \end{bmatrix}\begin{bmatrix} W_{71}(x_{13}, x_{14}) \\ W_{72}(x_{13}, x_{14}) \end{bmatrix} \\ &\quad - [\tilde{\theta}_{71}^T \quad \tilde{\theta}_{72}^T]\begin{bmatrix} \frac{1}{a_{71}}\dot{\theta}_{71} \\ \frac{1}{a_{72}}\dot{\theta}_{72} \end{bmatrix} - s_{13}^T\begin{bmatrix} \tilde{\vartheta}_{11}^T & 0 \\ 0 & \tilde{\vartheta}_{21}^T \end{bmatrix} \\ &\quad \times \begin{bmatrix} V_{11}(x_{13})\tau_1(t) \\ V_{21}(x_{13})\tau_1(t) \end{bmatrix} - [\tilde{\vartheta}_{11}^T \quad \tilde{\vartheta}_{21}^T]\begin{bmatrix} \frac{1}{A_{11}}\dot{\vartheta}_{11} \\ \frac{1}{A_{21}}\dot{\vartheta}_{21} \end{bmatrix} \\ &\quad - s_{13}^T\begin{bmatrix} \tilde{\vartheta}_{12}^T & 0 \\ 0 & \tilde{\vartheta}_{22}^T \end{bmatrix}\begin{bmatrix} V_{12}(x_{13})\tau_2(t) \\ V_{22}(x_{13})\tau_2(t) \end{bmatrix} - [\tilde{\vartheta}_{12}^T \quad \tilde{\vartheta}_{22}^T] \\ &\quad \times \begin{bmatrix} \frac{1}{a_{12}}\dot{\vartheta}_{12} \\ \frac{1}{a_{22}}\dot{\vartheta}_{22} \end{bmatrix} - s_{13}^T\begin{bmatrix} \tilde{\vartheta}_{12}^T & 0 \\ 0 & \tilde{\vartheta}_{22}^T \end{bmatrix} \\ &\quad \times \begin{bmatrix} V_{12}(x_{13})\tau_2(t) \\ V_{22}(x_{13})\tau_2(t) \end{bmatrix} - [\tilde{\vartheta}_{12}^T \quad \tilde{\vartheta}_{22}^T]\begin{bmatrix} \frac{1}{A_{12}}\dot{\vartheta}_{12} \\ \frac{1}{A_{22}}\dot{\vartheta}_{22} \end{bmatrix} + s_{13}^T \\ &\quad \times \left(-\begin{bmatrix} \varepsilon_{f_{71}} \\ \varepsilon_{f_{72}} \end{bmatrix} - k_{13} \operatorname{sign}(s_{13}) \right. \\ &\quad \left. - \begin{bmatrix} \varepsilon_{M_{11}}\tau_1(t) + \varepsilon_{M_{12}}\tau_2(t) \\ \varepsilon_{M_{21}}\tau_1(t) + \varepsilon_{M_{22}}\tau_2(t) \end{bmatrix} - \alpha_7(t)\right). \end{aligned} \tag{85}$$

By replacing (71) in (84) and (85), we get

$$\begin{aligned}\dot{V}_{2,2n+1} &= s_{2n+1}(-\varepsilon_{f_m} - k_{2n+1}\,\mathrm{sign}(s_{2n+1}) \\ &\quad - \varepsilon_{g_m}U_m(t) - \alpha_m(t)) \\ &= (-k_{2n+1}|s_{2n+1}| - \{\varepsilon_{f_m} + \varepsilon_{g_m}U_m(t) \\ &\quad + \alpha_m(t)\}s_{2n+1}),\end{aligned} \tag{86}$$

$$\begin{aligned}\dot{V}_{2,13} &= s_{13}^T\Bigg(-k_{13}\,\mathrm{sign}(s_{13}) \\ &\quad - \begin{bmatrix}-\varepsilon_{f_{71}} + \varepsilon_{M_{11}}\tau_1(t) + \varepsilon_{M_{12}}\tau_2(t) \\ -\varepsilon_{f_{72}} + \varepsilon_{M_{21}}\tau_1(t) + \varepsilon_{M_{22}}\tau_2(t)\end{bmatrix} - \alpha_7(t)\Bigg) \\ &= \Bigg(-(k_{13}\,\mathrm{sign}(s_{13}))^T s_{13} \\ &\quad - \begin{bmatrix}\varepsilon_{f_{71}} + \varepsilon_{M_{11}}\tau_1(t) + \varepsilon_{M_{12}}\tau_2(t) \\ \varepsilon_{f_{72}} + \varepsilon_{M_{21}}\tau_1(t) + \varepsilon_{M_{22}}\tau_2(t)\end{bmatrix}^T s_{13} \\ &\quad - \alpha_7^T(t)s_{13}\Bigg) \\ &= \Bigg(-k_{13}|s_{13}| - \begin{bmatrix}\varepsilon_{f_{71}} + \varepsilon_{M_{11}}\tau_1(t) + \varepsilon_{M_{12}}\tau_2(t) \\ \varepsilon_{f_{72}} + \varepsilon_{M_{21}}\tau_1(t) + \varepsilon_{M_{22}}\tau_2(t)\end{bmatrix}^T s_{13} \\ &\quad - \alpha_7^T(t)s_{13}\Bigg).\end{aligned} \tag{87}$$

Ultimately, it may be determined that $\dot{V}_{2,2n+1} < 0$ and $\dot{V}_{2,13}<0$ by selecting the discontinuous control gains as

$$\begin{aligned}k_{13} &= \mathrm{diag}\{k_{131}, k_{132}\} \geq [\mathrm{diag}\{(D_{\alpha 7} + \eta_{13}), (D_{\alpha 7} \\ &\quad + \eta_{13})\}] + [\mathrm{diag}\{|\varepsilon_{f_{71}} + \varepsilon_{M_{11}}\tau_1(t) + \varepsilon_{M_{12}}\tau_2(t)|, \\ &\quad \times |\varepsilon_{f_{72}} + \varepsilon_{M_{21}}\tau_1(t) + \varepsilon_{M_{22}}\tau_2(t)|\}]\end{aligned}$$

and $k_{2n+1} \geq D_{\alpha m} + |\varepsilon_{f_m} + \varepsilon_{g_m}U_m(t)| + \eta_{2n+1}$. As a result, even in the event of actuator failures and model uncertainty, the suggested control rule may preserve system performance. □

6. Disturbance Observer Based on Type-2 Fuzzy Adaptive Sliding Mode Control Strategy

To accommodate for the unidentified uncertainties, the selection of the discontinuous control gain should be such that:

$$\begin{aligned}k_{13} &= \mathrm{diag}\{k_{131}, k_{132}\} \geq [\mathrm{diag}\{(D_{\alpha 7} + \eta_{13}), (D_{\alpha 7} \\ &\quad + \eta_{13})\}] + [\mathrm{diag}\{|\varepsilon_{f_{71}} + \varepsilon_{M_{11}}\tau_1(t) + \varepsilon_{M_{12}}\tau_2(t)|, \\ &\quad \times |\varepsilon_{f_{72}} + \varepsilon_{M_{21}}\tau_1(t) + \varepsilon_{M_{22}}\tau_2(t)|\}]\end{aligned}$$

and $k_{2n+1} \geq D_{\alpha m} + |\varepsilon_{f_m} + \varepsilon_{g_m}U_m(t)| + \eta_{2n+1}$ as determined in the previous design. However, it is important to note that this choice may result in unanticipated control chattering if the disturbances are quite high. This section introduces the creation of a nonlinear disturbance observer to enhance the reduction of the discontinuous control gain. The observer is then included in the previously established adaptive sliding mode control to adjust for actuator defects, model errors and external disturbances.

Assumption 3 ([31,65]). The disturbance's time derivative in (27) is bounded and fulfills $\dot{\alpha}_m(t) = 0$ and $\dot{\alpha}_7(t) = 0$.

In order to approximate the value of the unknown disturbances $\alpha_m(t)$ and $\alpha_7(t)$, a nonlinear disturbance observer is formulated as per Refs. [68, 69]:

$$\begin{cases}\dot{z}_m = -\kappa_m z_m - \kappa_m(\kappa_m x_{2m} + f_m(X) + g_m(X)U_m(t)), \\ \hat{\alpha}_m(t) = z_m + \kappa_m x_{2m},\end{cases} \tag{88}$$

$$\begin{cases}\dot{z}_7 = -\kappa_7 z_7 - \kappa_7(\kappa_7 x_{14} + f_7(x_{13}, x_{14}) + M^{-1}(x_{13})\tau(t)), \\ \hat{\alpha}_7(t) = z_7 + \kappa_7 x_{14}.\end{cases} \tag{89}$$

The variables z_m and z_7 represents the internal state of the nonlinear observer, while κ_m and

$$\kappa_7 = \begin{bmatrix}\kappa_{71} & 0 \\ 0 & \kappa_{72}\end{bmatrix} = \mathrm{diag}(\kappa_{71}, \kappa_{72})$$

denotes the gain of the nonlinear disturbance observer.

The disturbances estimation errors can be described as the difference between the actual disturbances and the estimated disturbances as

$$\tilde{\alpha}_m(t) = \alpha_m(t) - \hat{\alpha}_m(t), \tag{90}$$

$$\tilde{\alpha}_7(t) = \alpha_7(t) - \hat{\alpha}_7(t). \tag{91}$$

Subsequently, by invoking Assumption 1 and combing (27) and (88) through (91) the time derivative of the disturbances estimation error can be described by

$$\begin{aligned}\dot{\tilde{\alpha}}_m(t) &= \dot{\alpha}_m(t) - \dot{\hat{\alpha}}_m(t) \\ &= -\dot{z}_m - \kappa_m\dot{x}_{2m} \\ &= \kappa_m(\hat{\alpha}_m(t) - \kappa_m x_{2m}) + \kappa_m(\kappa_m x_{2m} \\ &\quad + f_m(X) + g_m(X)U_m(t)) \\ &\quad - \kappa_m(f_m(X) + g_m(X)U_m(t) + \alpha_m(t)) \\ &= -\kappa_m\tilde{\alpha}_m(t),\end{aligned} \tag{92}$$

$$\begin{aligned}\dot{\tilde{\alpha}}_7(t) &= \dot{\alpha}_7(t) - \dot{\hat{\alpha}}_7(t) \\ &= -\dot{z}_7 - \kappa_7\dot{x}_{14} \\ &= \kappa_7(\hat{\alpha}_7(t) - \kappa_7 x_{14}) + \kappa_7(\kappa_7 x_{14} + f_7(x_{13}, x_{14}) \\ &\quad + M^{-1}(x_{13})\tau(t)) \\ &\quad - \kappa_7(f_7(x_{13}, x_{14}) + M^{-1}(x_{13})\tau(t) + \alpha_7(t)) \\ &= -\kappa_7\tilde{\alpha}_7(t).\end{aligned} \tag{93}$$

By using the adaptive sliding mode control law obtained in Eq. (70), which does not take into account the unknown disturbances in order to produce the continuous control components, the composite control laws may be generated by including the estimated disturbances $\hat{\alpha}_m(t)$ and $\hat{\alpha}_7(t)$ expressed as

$$\begin{cases} U_m(t) = \frac{1}{\hat{g}_m(X)}(\ddot{x}_{(2n+1)d} + \lambda_{2n+1}(\dot{x}_{(2n+1)d} \\ \qquad - \dot{x}_{2n+1}) - \hat{F}_m(X) - \hat{\alpha}_m(t) \\ \qquad + k_m \operatorname{sign}(s_{2n+1})), \\ \tau(t) = \hat{M}(x_{13})\{\ddot{x}_{13d} + \lambda_{13}(\dot{x}_{13d} - \dot{x}_{13}) \\ \qquad - \hat{F}_7(x_{13}, x_{14}) - \hat{\alpha}_7(t) + k_{13} \operatorname{sign}(s_{13})\}. \end{cases} \tag{94}$$

Theorem 3. *Consider a nonlinear system* (27), *including actuator defects, model uncertainties and unknown disturbances. Using the feedback control laws in* (94) *and disturbance observer* (88) *and* (89) *adjusted by* (62) *through* (65) *and* (71), *the desired sliding movement is maintained despite external disturbances, actuator faults and model uncertainties. The discontinuous control gains are selected as*

$$k_{13} = \operatorname{diag}\{k_{131}, k_{132}\} \geq [\operatorname{diag}\{(E_{\alpha 7} + \eta_{13}), (E_{\alpha 7} + \eta_{13})\}] + [\operatorname{diag}\{|\varepsilon_{f_{71}} + \varepsilon_{M_{11}}\tau_1(t) + \varepsilon_{M_{12}}\tau_2(t)|, \times |\varepsilon_{f_{72}} + \varepsilon_{M_{21}}\tau_1(t) + \varepsilon_{M_{22}}\tau_2(t)|\}]$$

and $k_{2n+1} \geq E_{\alpha m} + |\varepsilon_{f_m} + \varepsilon_{g_m} U_m(t)| + \eta_{2n+1}$.

Proof. Define the following Lyapunov candidate functions as

$$V_{3,2n+1} = \frac{1}{2}s_{2n+1}^2 + \tilde{\alpha}_m^2 + \frac{1}{a_{1m}}\tilde{\theta}_m^T\tilde{\theta}_m + \frac{1}{a_{2m}} \times \tilde{\vartheta}_m^T\tilde{\vartheta}_m, \quad n = 0, \dots, 5 \; m = 1, \dots, 6, \tag{95}$$

$$V_{3,13} = \frac{1}{2}s_{13}^T s_{13} + \frac{1}{2}\tilde{\alpha}_7^T\tilde{\alpha}_7 + \frac{1}{a_{71}}\tilde{\theta}_{71}^T\tilde{\theta}_{71} + \frac{1}{a_{72}}\tilde{\theta}_{72}^T\tilde{\theta}_{72} + \frac{1}{a_{11}}\tilde{\vartheta}_{11}^T\tilde{\vartheta}_{11} + \frac{1}{a_{12}}\tilde{\vartheta}_{12}^T\tilde{\vartheta}_{12} + \frac{1}{a_{21}}\tilde{\vartheta}_{21}^T\tilde{\vartheta}_{21} + \frac{1}{a_{22}}\tilde{\vartheta}_{22}^T\tilde{\vartheta}_{22}. \tag{96}$$

Then, the temporal derivative of the chosen Lyapunov candidate functions in (95) and (96) can be expressed as

$$\begin{aligned} \dot{V}_{3,2n+1} &= s_{2n+1}\dot{s}_{2n+1} + \tilde{\alpha}_m\dot{\tilde{\alpha}}_m + \frac{1}{a_{1m}}\tilde{\theta}_m^T\dot{\tilde{\theta}}_m + \frac{1}{a_{2m}} \times \tilde{\vartheta}_m^T\dot{\tilde{\vartheta}}_m \qquad (97) \\ &= s_{2n+1}([-W_m^T(X_m)\tilde{\theta}_m - \varepsilon_{f_m}] - k_{2n+1} \times \operatorname{sign}(s_{2n+1}) + \{-V_m^T(X_m)\tilde{\vartheta}_m - \varepsilon_{g_m}\}U_m(t) - \tilde{\alpha}_m) - \frac{1}{a_{1m}}\tilde{\theta}_m^T\dot{\theta}_m - \frac{1}{a_{2m}}\tilde{\vartheta}_m^T\dot{\vartheta}_m - \kappa_m\tilde{\alpha}_m^2 \\ &= \tilde{\theta}_m^T(-s_{2n+1}W_m(X_m) - \frac{1}{a_{1m}}\dot{\theta}_m) + \tilde{\vartheta}_m^T \times (-s_{2n+1}V_m(X_m)U_m(t) - \frac{1}{a_{2m}}\dot{\vartheta}_m) \\ &\quad + s_{2n+1}(-\varepsilon_{f_m} - k_{2n+1}\operatorname{sign}(s_{2n+1}) - \varepsilon_{g_m}U_m(t) - \tilde{\alpha}_m) - \kappa_m\tilde{\alpha}_m^2, \end{aligned} \tag{98}$$

$$\dot{V}_{3,13} = s_{13}^T\dot{s}_{13} + \tilde{\alpha}_7^T\dot{\tilde{\alpha}}_7 + \frac{1}{a_{71}}\tilde{\theta}_{71}^T\dot{\tilde{\theta}}_{71} + \frac{1}{a_{72}}\tilde{\theta}_{72}^T\dot{\tilde{\theta}}_{72} + \frac{1}{a_{11}}\tilde{\vartheta}_{11}^T\dot{\tilde{\vartheta}}_{11} + \frac{1}{a_{12}}\tilde{\vartheta}_{12}^T\dot{\tilde{\vartheta}}_{12} + \frac{1}{a_{21}}\tilde{\vartheta}_{21}^T\dot{\tilde{\vartheta}}_{21} + \frac{1}{a_{22}}\tilde{\vartheta}_{22}^T\dot{\tilde{\vartheta}}_{22} \tag{99}$$

$$\begin{aligned} &= s_{13}^T\left[\begin{bmatrix} -W_{71}^T(x_{13}, x_{14})\tilde{\theta}_{71} - \varepsilon_{f_{71}} \\ -W_{72}^T(x_{13}, x_{14})\tilde{\theta}_{72} - \varepsilon_{f_{72}} \end{bmatrix} - k_{13}\operatorname{sign}(s_{13}) + \begin{bmatrix} -V_{11}^T(x_{13})\tilde{\vartheta}_{11} - \varepsilon_{M_{11}} & -V_{12}^T(x_{13})\tilde{\vartheta}_{12} - \varepsilon_{M_{12}} \\ -V_{21}^T(x_{13})\tilde{\vartheta}_{21} - \varepsilon_{M_{21}} & -V_{22}^T(x_{13})\tilde{\vartheta}_{22} - \varepsilon_{M_{22}} \end{bmatrix}\tau(t) - \tilde{\alpha}_7(t)\right] \\ &\quad - \frac{1}{a_{71}}\tilde{\theta}_{71}^T\dot{\theta}_{71} - \frac{1}{a_{72}}\tilde{\theta}_{72}^T\dot{\theta}_{72} - \frac{1}{a_{11}}\tilde{\vartheta}_{11}^T\dot{\vartheta}_{11} - \frac{1}{a_{12}}\tilde{\vartheta}_{12}^T\dot{\vartheta}_{12} - \frac{1}{a_{21}}\tilde{\vartheta}_{21}^T\dot{\vartheta}_{21} - \frac{1}{a_{22}}\tilde{\vartheta}_{22}^T\dot{\vartheta}_{22} + \tilde{\alpha}_7^T\dot{\tilde{\alpha}}_7 \\ &= -s_{13}^T\begin{bmatrix} \tilde{\theta}_{71}^T & 0 \\ 0 & \tilde{\theta}_{72}^T \end{bmatrix}\begin{bmatrix} W_{71}(x_{13}, x_{14}) \\ W_{72}(x_{13}, x_{14}) \end{bmatrix} - \begin{bmatrix} \tilde{\theta}_{71}^T & \tilde{\theta}_{72}^T \end{bmatrix}\begin{bmatrix} \frac{1}{a_{71}}\dot{\theta}_{71} \\ \frac{1}{a_{72}}\dot{\theta}_{72} \end{bmatrix} - s_{13}^T \\ &\quad \times \begin{bmatrix} \tilde{\vartheta}_{11}^T & 0 \\ 0 & \tilde{\vartheta}_{21}^T \end{bmatrix}\begin{bmatrix} V_{11}(x_{13})\tau_1(t) \\ V_{21}(x_{13})\tau_1(t) \end{bmatrix} - \begin{bmatrix} \tilde{\vartheta}_{11}^T & \tilde{\vartheta}_{21}^T \end{bmatrix}\begin{bmatrix} \frac{1}{A_{11}}\dot{\vartheta}_{11} \\ \frac{1}{A_{21}}\dot{\vartheta}_{21} \end{bmatrix} - s_{13}^T\begin{bmatrix} \tilde{\vartheta}_{12}^T & 0 \\ 0 & \tilde{\vartheta}_{22}^T \end{bmatrix} \\ &\quad \begin{bmatrix} V_{12}(x_{13})\tau_2(t) \\ V_{22}(x_{13})\tau_2(t) \end{bmatrix} - \begin{bmatrix} \tilde{\vartheta}_{12}^T & \tilde{\vartheta}_{22}^T \end{bmatrix}\begin{bmatrix} \frac{1}{a_{12}}\dot{\vartheta}_{12} \\ \frac{1}{a_{22}}\dot{\vartheta}_{22} \end{bmatrix} \end{aligned}$$

$$
\begin{aligned}
&- s_{13}^T \begin{bmatrix} \tilde{\vartheta}_{12}^T & 0 \\ 0 & \tilde{\vartheta}_{22}^T \end{bmatrix} \begin{bmatrix} V_{12}(x_{13})\tau_2(t) \\ V_{22}(x_{13})\tau_2(t) \end{bmatrix} \\
&- \begin{bmatrix} \tilde{\vartheta}_{12}^T & \tilde{\vartheta}_{22}^T \end{bmatrix} \begin{bmatrix} \frac{1}{A_{12}}\dot{\vartheta}_{12} \\ \frac{1}{A_{22}}\dot{\vartheta}_{22} \end{bmatrix} \\
&+ s_{13}^T \left(- \begin{bmatrix} \varepsilon_{f_{71}} \\ \varepsilon_{f_{72}} \end{bmatrix} - k_{13}\,\mathrm{sign}(s_{13}) \right. \\
&\left. - \begin{bmatrix} \varepsilon_{M_{11}}\tau_1(t) + \varepsilon_{M_{12}}\tau_2(t) \\ \varepsilon_{M_{21}}\tau_1(t) + \varepsilon_{M_{22}}\tau_2(t) \end{bmatrix} - \tilde{\alpha}_7(t) \right) \\
&- \tilde{\alpha}_7^T(\kappa_7\tilde{\alpha}_7(t)). \qquad (100)
\end{aligned}
$$

By replacing (71) in (98) and (100), we get

$$
\begin{aligned}
\dot{V}_{3,2n+1} &= s_{2n+1}(-\varepsilon_{f_m} - k_{2n+1}\,\mathrm{sign}(s_{2n+1}) - \varepsilon_{g_m} \\
&\quad \times U_m(t) - \tilde{\alpha}_m) - \kappa_m\tilde{\alpha}_m^2 \\
&= (-k_{2n+1}|s_{2n+1}| - \{\varepsilon_{f_m} + \varepsilon_{g_m}U_m(t) \\
&\quad + \tilde{\alpha}_m\}s_{2n+1}) - \kappa_m\tilde{\alpha}_m^2, \qquad (101)
\end{aligned}
$$

$$
\begin{aligned}
\dot{V}_{3,13} &= s_{13}^T \left(-k_{13}\,\mathrm{sign}(s_{13}) \right. \\
&\quad \left. - \begin{bmatrix} -\varepsilon_{f_{71}} + \varepsilon_{M_{11}}\tau_1(t) + \varepsilon_{M_{12}}\tau_2(t) \\ -\varepsilon_{f_{72}} + \varepsilon_{M_{21}}\tau_1(t) + \varepsilon_{M_{22}}\tau_2(t) \end{bmatrix} - \tilde{\alpha}_7 \right) \\
&\quad - \tilde{\alpha}_7^T(\kappa_7\tilde{\alpha}_7(t)) \\
&= \left(-(k_{13}\,\mathrm{sign}(s_{13}))^T s_{13} \right. \\
&\quad - \begin{bmatrix} \varepsilon_{f_{71}} + \varepsilon_{M_{11}}\tau_1(t) + \varepsilon_{M_{12}}\tau_2(t) \\ \varepsilon_{f_{72}} + \varepsilon_{M_{21}}\tau_1(t) + \varepsilon_{M_{22}}\tau_2(t) \end{bmatrix}^T \\
&\quad \left. \times s_{13} - \tilde{\alpha}_7^T s_{13} \right) - \tilde{\alpha}_7^T(\kappa_7\tilde{\alpha}_7(t)) \\
&= \left(-k_{13}|s_{13}| \right. \\
&\quad - \begin{bmatrix} \varepsilon_{f_{71}} + \varepsilon_{M_{11}}\tau_1(t) + \varepsilon_{M_{12}}\tau_2(t) \\ \varepsilon_{f_{72}} + \varepsilon_{M_{21}}\tau_1(t) + \varepsilon_{M_{22}}\tau_2(t) \end{bmatrix}^T \\
&\quad \left. \times s_{13} - \tilde{\alpha}_7^T s_{13} \right) - \tilde{\alpha}_7^T(\kappa_7\tilde{\alpha}_7(t)). \qquad (102)
\end{aligned}
$$

Ultimately, it may be determined that $\dot{V}_{3,2n+1}$<0 and $\dot{V}_{3,13} < 0$ by selecting the discontinuous control gains as

$$
\begin{aligned}
k_{13} &= \mathrm{diag}\{k_{131}, k_{132}\} \geq [\mathrm{diag}\{(E_{\alpha 7} + \eta_7), (E_{\alpha 7} \\
&\quad + \eta_7)\}] + [\mathrm{diag}\{|\varepsilon_{f_{71}} + \varepsilon_{M_{11}}\tau_1(t) + \varepsilon_{M_{12}}\tau_2(t)|, \\
&\quad \times |\varepsilon_{f_{72}} + \varepsilon_{M_{21}}\tau_1(t) + \varepsilon_{M_{22}}\tau_2(t)|\}]
\end{aligned}
$$

and $k_{2n+1} \geq E_{\alpha m} + |\varepsilon_{f_m} + \varepsilon_{g_m}U_m(t)| + \eta_{2n+1}$, where $O_{\alpha_7} = \mathrm{diag}\{E_{\alpha_7}, E_{\alpha_7}\}$ and $E_{\alpha m}$ are the upper bound of the disturbance estimation errors. As a result, even in the event of actuator failures and model uncertainty, the suggested control rule may preserve system performance. □

Remark 3. Due to the accurate assessment of unknown disturbances by the disturbance observer, the upper limit of the disturbance estimation errors $E_{\alpha m}$ and O_{α_7} is much less than the upper limit of the real disturbances D_{α_7} and $H_{\alpha_7} = \mathrm{diag}\{D_{\alpha_7}, D_{\alpha_7}\}$. Hence, the discontinuous control gains used in the control laws (94) presented in this section are significantly less in comparison to the ones utilized in the control law created in (70). By implementing the control laws described in Eq. (94), the chattering issue in sliding mode control can be partially mitigated. These control laws also have the ability to overcome external disturbances, actuator faults and model uncertainties.

Remark 4. Table 2 shows a comparison study conducted to demonstrate the efficacy of the proposed control strategy compared to related works and provide the most comprehensive visibility.

7. Simulation Results and Discussions

In this section, a number of simulated case studies and tests are used to assess the proposed type-2 fuzzy adaptive sliding mode control (PT2FASMC) technique for MMUAV's capability in handling actuator defects, model uncertainties and external disturbances. The physical parameters of the MMUAV under study are shown in Table 3.

To provide a fair comparison and showcase the benefits of the proposed control strategy, we will also examine the performance of a conventional sliding mode control (CSMC). The control parameters depicted in Table 4 are carefully selected using a trial-and-error method to ensure optimal performance. In addition, to optimize the computation time of the suggested control method, just three Type 2 membership functions are used for each input variable in the fuzzy systems being studied.

To verify the efficacy of the suggested control technique, two scenarios are presented.

Remark 5. The simulations are executed on a DELL computer equipped with MATLAB/Simulink software. It includes a 3.0 GHz processor, 8 GB of RAM and a 500 GB SSD.

Scenario 1. Step trajectory tracking for the UAV and manipulator in the presence of parametric uncertainty, actuator faults and external disturbances.

Table 2. Comparative study.

Proposed control scheme	Other control approaches	Corresponding papers
The closed-loop system exhibits global asymptotic stability, and the tracking error converges exponentially to the origin owing to the accurate approximation based on type-2 fuzzy systems	The closed-loop system exhibits uniform ultimate boundedness (UUB) stability, and the tracking error converges exponentially just to a compact set, attributable to the residual components from estimation	[10, 13, 37, 49, 56]
Considers four types of actuator defects: bias, drift, accuracy loss and effectiveness loss	The applicability of these methods is restricted to one or two types of actuator defects	[46, 47, 49, 50, 52]
A nonlinear disturbance observer aims to compensate for external disturbances, while the suggested adaptive type-2 fuzzy systems are used to compensate for actuator defects and model uncertainties, respectively	The disturbance is characterized as an exogenous neutral, stable system, or it has been approximated accordingly. Authors assumed that the time-derivative of the disturbances must remain bounded	[30, 36, 44]
The absence of a fault detection and isolation (FDI) module results in the controller automatically managing actuator faults by adjusting its operations to mitigate the negative impacts. Additionally, the time delay associated with detection is eliminated	The FDI module is utilized for fault detection and isolation	[14]
No information is required for actuator malfunctions since the controller updates live to mitigate the impact	Need actuator fault models	[50, 53, 54]
It is assumed that the control gain is an unknown nonlinear function	The control gain is a straightforward constant that restricts the scope of the systems under consideration	[51, 52, 55, 57]

Table 3. Physical parameters of the MMUAV [62].

Parameters	Values	Description
m	3.2 Kg	UAV mass
m_1	0.2 Kg	Mass of link 1 of the manipulator
m_2	0.22 Kg	Mass of link 2 of the manipulator
I_x, I_y, I_z	28.7×10^{-3} Kg · m^2, 20.6×10^{-3} Kg · m^2, 20.6×10^{-3} Kg · m^2	UAV inertia
I_1, I_2	8.6×10^{-3} Kg · m^2, 7.8×10^{-3} Kg · m^2	Links inertias of the manipulator
l	0.35 m	UAV arm length
l_1, l_2	0.21 m, 0.21 m	Manipulator links lengths
g	9.81 m/s^2	Gravity
c_v	0.06	Torque gain related to the generated torque by six rotors.

Table 4. Control parameters.

Parameters	Values
λ_{2n+1} for $n = 0, \ldots, 5$	1
λ_{13}	diag[0.8, 0.1]
k_{2n+1} for $n = 0, \ldots, 5$	1
k_{13}	diag[20, 20]
η_{2n+1} for $n = 0, \ldots, 5$	0.1
η_{13}	0.1
a_{1m} for $m = 1, \ldots, 6$	100
a_{71}	100
a_{72}	100
A_{11}	150
A_{12}	150
A_{21}	150
A_{22}	150
κ_m for $m = 1, \ldots, 6$	120
κ_7	diag[120, 120]

In this Scenario 1, actuator faults in MMUAV are generated using the additive and multiplicative faults model described in Table 1, where the loss of control effectiveness faults are injected to U_1, U_2, U_3 and U_4 at $t = 25$ s, $t = 50$ s, $t = 75$ s and $t = 100$ s, respectively. Subsequently, similar faults are intentionally introduced to $\tau(t) = [\tau_1(t)\tau_2(t)]^T$ at $t = 125$ s. In order to assess the robustness of the suggested control approach against uncertainties in the model parameters, we are considering a 90% variation in the mass m, 70% variation in the mass m_1 and 70% variation in the mass m_2 at $t = 60$ s. Besides, the equations of the MMUAV model take into consideration the external disturbances. Interruptions can occur when the MMUAV is flying outside due to wind gusts. Consequently, the disturbing expressions are considered at time $t = 20$ s as sinusoidal waves of different frequencies, given as [70]

$$\begin{cases} \alpha_1(t) = 0.5\cos(0.4t) + 1, \quad \alpha_2(t) = 0.5\cos(0.5t) + 1, \\ \alpha_3(t) = 0.5\cos(0.7t) + 1, \\ \alpha_4(t) = 0.5\cos(0.7t) + 0.7\cos(0.3t), \\ \alpha_5(t) = -0.08\cos(0.1013t - 3.043) + 0.1\sin(0.448t \\ \qquad - 13.464) + 0.05\sin(1.5708t - 15\pi), \\ \alpha_6(t) = 0.05\cos(0.4t) + 0.05\cos(0.7t), \\ \alpha_7(t) = \left[5\cos(0.4t) + 1 \quad 5\cos(0.4t) + 1\right]^T. \end{cases} \tag{103}$$

The trajectory tracking of the MMUAV is shown in Figs. 6 and 7, when there are numerous actuator problems, uncertainties and external disturbances. The PT2FASMC is able to adequately handle these faults such that the tracking performance remains unchanged and the tracking errors eventually converge to zero. In reality, it is not possible to provide appropriate trajectory tracking for the provided reference command using CSMC in the event of actuator faults, uncertainties and external disturbances. In addition, the CSMC tracks the reference command with considerable oscillations as presented in Fig. 6, and it has the weakest tracking performance once faults arise. Due to the fact that yaw and height motion is affected by four actuators, when faults occur in the actuators, $(x, y, z, \psi, q_1, q_2)$ positions are more affected than (φ, θ). Also, as shown in Figs. 8–10, the CSMC requires greater control efforts than the PT2FASMC to keep the system tracking performance stable, since the discontinuous control gain increases. Chattering from the controls may potentially cause the system to become unstable by triggering unwanted dynamics.

The capability of the developed disturbance observer is shown in Figs. 11 and 12, which illustrate the estimated terms of external disturbances. The global trajectory in 3D is depicted in Fig. 13. In Figs. 14(a)–14(d) and 15(a)–15(d), we see an asymptotic convergence for the sliding surfaces toward the origin of the proposed PT2FASMC. In contrast to the CSMC, there is a divergence of sliding surfaces.

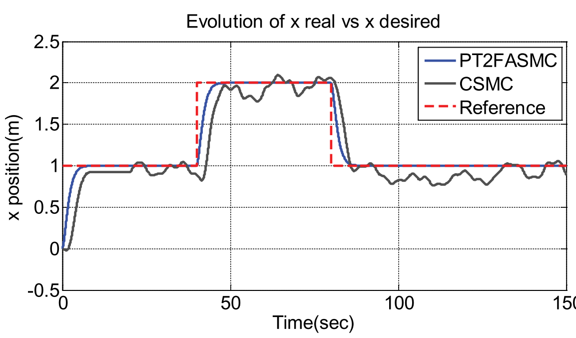

(a)

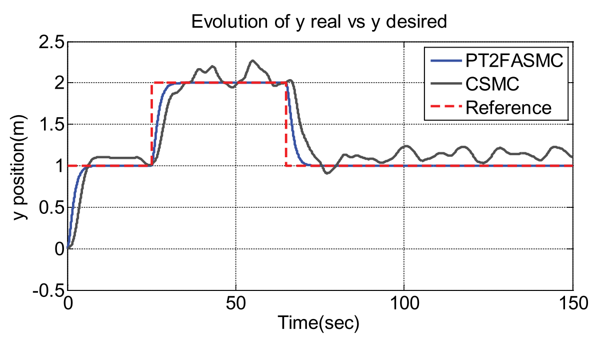

(b)

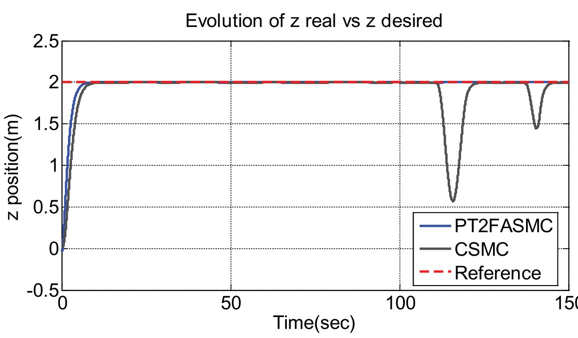

(c)

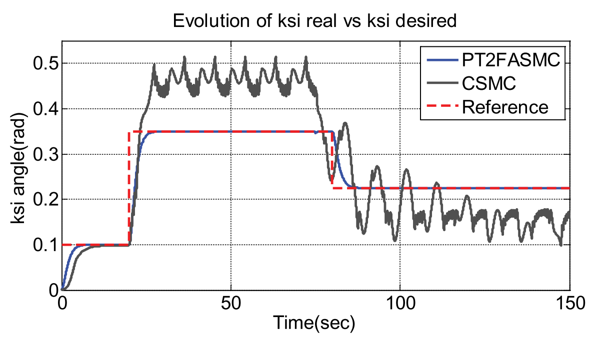

(d)

Fig. 6. (x, y, z) positions and yaw angle (ψ) outputs of the UAV in the presence actuator faults, uncertainties and external disturbances (Scenario 1).

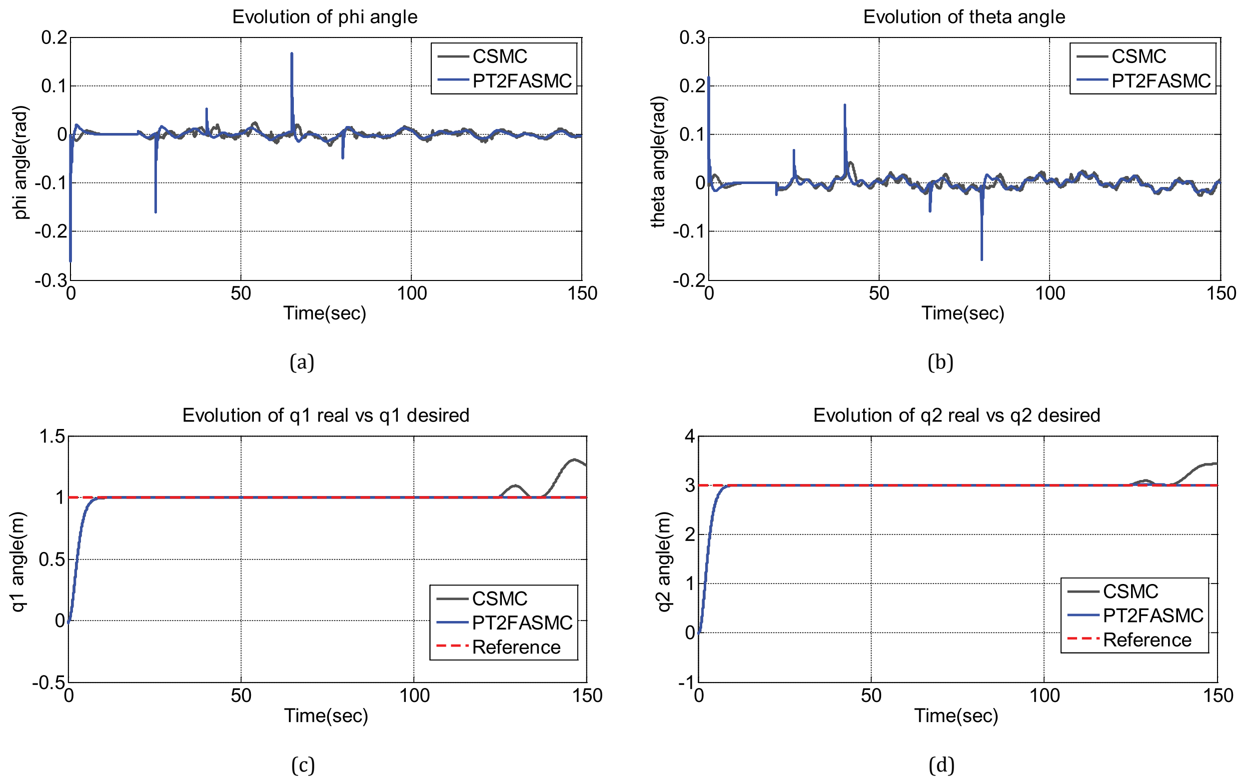

Fig. 7. Roll and pitch angles (φ, θ) of the UAV and q_1 and q_2 angles of the outputs manipulator in the presence actuator faults, uncertainties and external disturbances (Scenario 1).

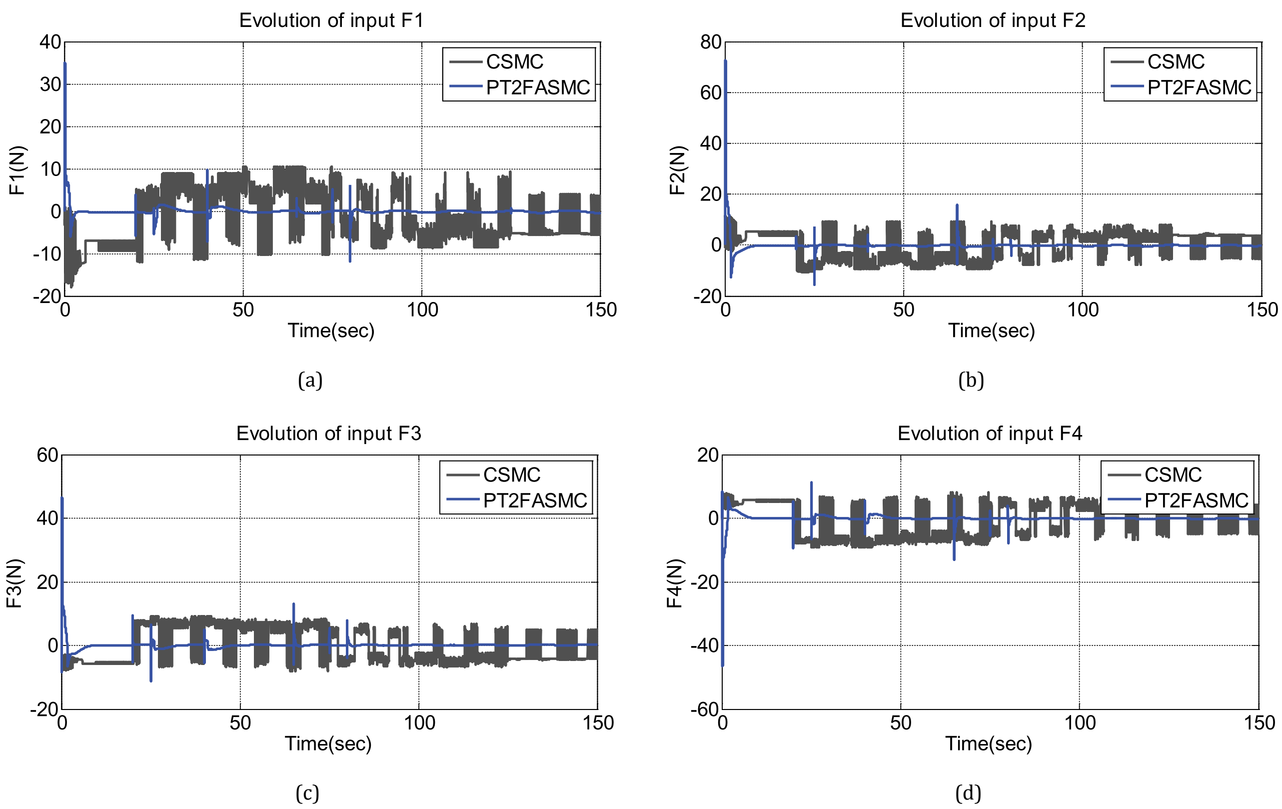

Fig. 8. The six input forces of the UAV (Scenario 1).

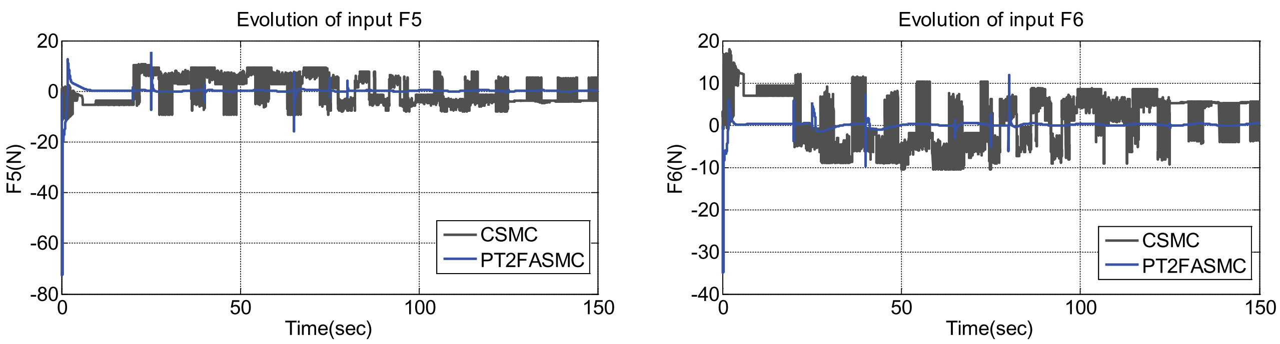

(e) (f)

Fig. 8. (*Continued*)

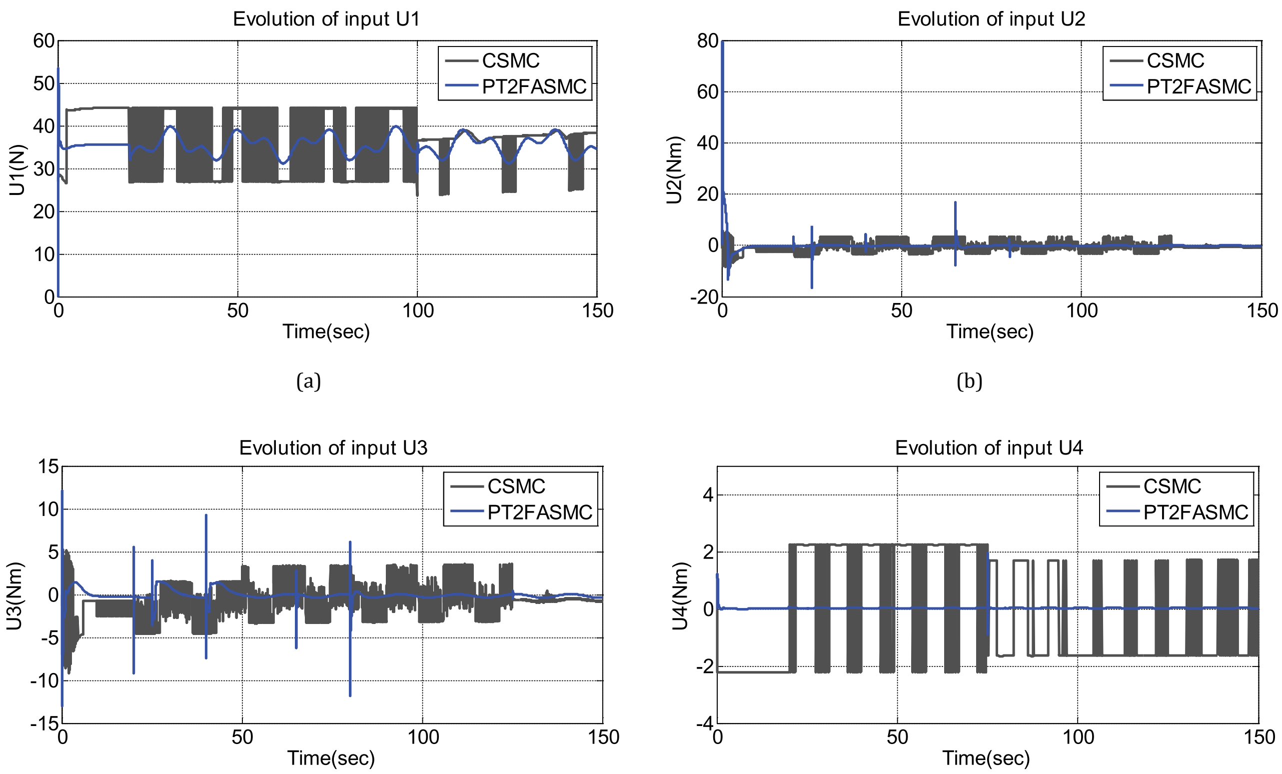

(a) (b) (c) (d)

Fig. 9. Control inputs of the UAV (Scenario 1).

Scenario 2. Sine trajectory tracking for the UAV and manipulator in the presence of parametric uncertainty, actuator faults and external disturbances.

In Scenario 2, a sinusoidal desired trajectory is considered as [70]: $x_d = 0.5\cos(\frac{\pi t}{20})$, $y_d = 0.5\sin(\frac{\pi t}{20})$, $z_d = 3 - 2\cos(\frac{\pi t}{20})$, $\psi_d = 0.5$, $q_{1d} = 12\cos(\frac{t}{3}) + 11\cos(\frac{\pi}{4})$ and $q_{2d} = 12\sin(\frac{t}{3}) + 11\sin(\frac{\pi}{4})$, the actuator faults in the MMUAV are created using the additive and multiplicative faults model outlined in Table 1. Specifically, loss of control effectiveness faults are introduced to U_1, U_2, U_3 and U_4 at certain times: $t = 5$ s, $t = 10$ s, $t = 15$ s and $t = 20$ s, respectively. Following that, a deliberate introduction of a similar fault is made to $\tau(t) = [\tau_1(t)\ \tau_2(t)]^T$ at $t = 20$ s. To evaluate the effectiveness of the proposed control method in dealing with uncertainties in the model parameters, we will examine a 90% change in the mass m, a 70% change in the

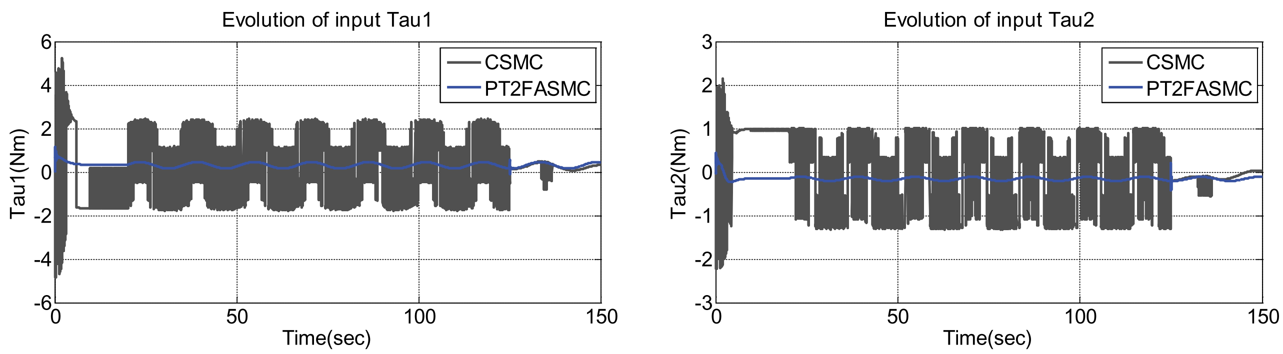

(a) (b)

Fig. 10. Torque control inputs of the manipulator (Scenario 1).

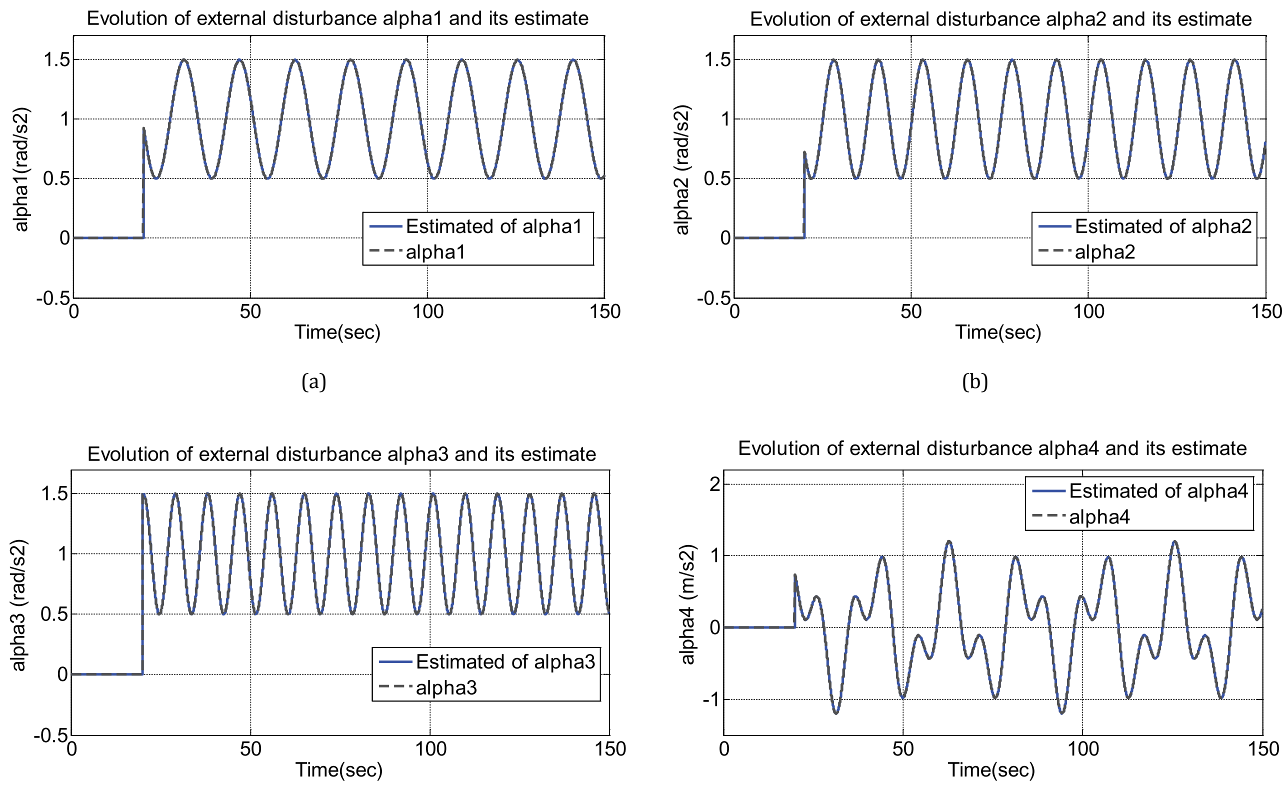

(a) (b) (c) (d)

Fig. 11. $\alpha_1, \alpha_2, \alpha_3$ and α_4 estimation (Scenario 1).

mass m_1 and a 70% change in the mass m_2 at $t = 5$ s. In addition, the unsettling expressions in (103) has been added at $t = 20$ s. The tracking performance of the MMUAV helicopter in the faulty situation is shown in Figs. 16 and 17. The PT2FASMC can keep the system working well even when there are multiple actuator faults, parametric uncertainties and disturbances from the outside. This is achieved through the implementation of a designed disturbance observer and adaptive control schemes. Additionally, the PT2FASMC is able to suppress control chattering by maintaining a small discontinuous control gain, as depicted in Figs. 18–20. However, when actuator problems happen, the CSMC cannot only make sure that the desired reference command is tracked if they are focused on dealing with parametric uncertainties

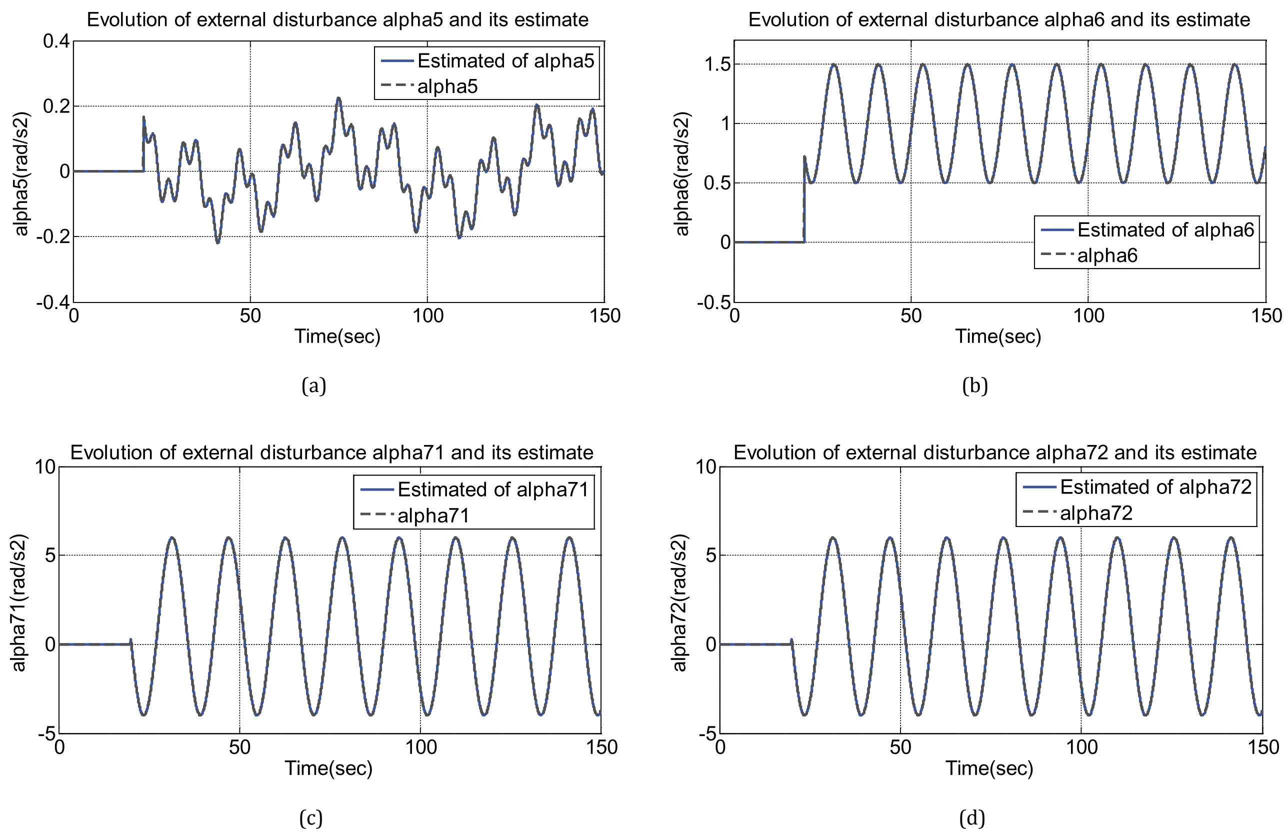

Fig. 12. α_5, α_6, α_{71} and α_{72} estimation (Scenario 1).

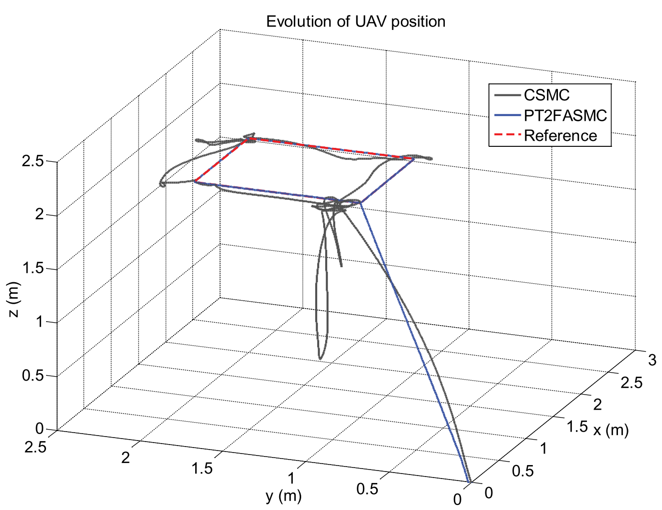

Fig. 13. 3D Position tracking result of the UAV.

and outside disturbances. Figures 18–20 display the control inputs of the actuators using the two techniques. Control chattering happens in the CSMC when a discontinuous control approach is used too much to deal with actuator problems, parametric uncertainties and disturbances from the outside. Moreover, the introduction of additional uncertain elements into the system exacerbates the oscillation of the system output via CSMC.

Figures 21 and 22 depict the estimated components of external disturbances, showing the effectiveness of the constructed disturbance observer. Figure 23 illustrates the global path in three dimensions. Figures 24(a)–24(d) and 25(a)–25(d) illustrate an asymptotic convergence of the sliding surfaces toward the origin of the proposed PT2FASMC. Unlike the CSMC, there exists a divergence of sliding surfaces.

To examine the two control laws, we define criteria J_1 and J_2 in (104) and (105) according to the applied control. They are considered energy criteria to justify the chattering mitigation:

$$J_1 = \frac{1}{2}\sum_{k=1}^{p} U^T U, \tag{104}$$

$$J_2 = \frac{1}{2}\sum_{k=1}^{p} \tau^T \tau. \tag{105}$$

The CSMC requires significant energy, as seen by criterions J_1 and J_2 in Table 5. In addition, as we said previously, this control is at high frequencies, which gives rise to chattering. In addition, the calculation of the equivalent control requires

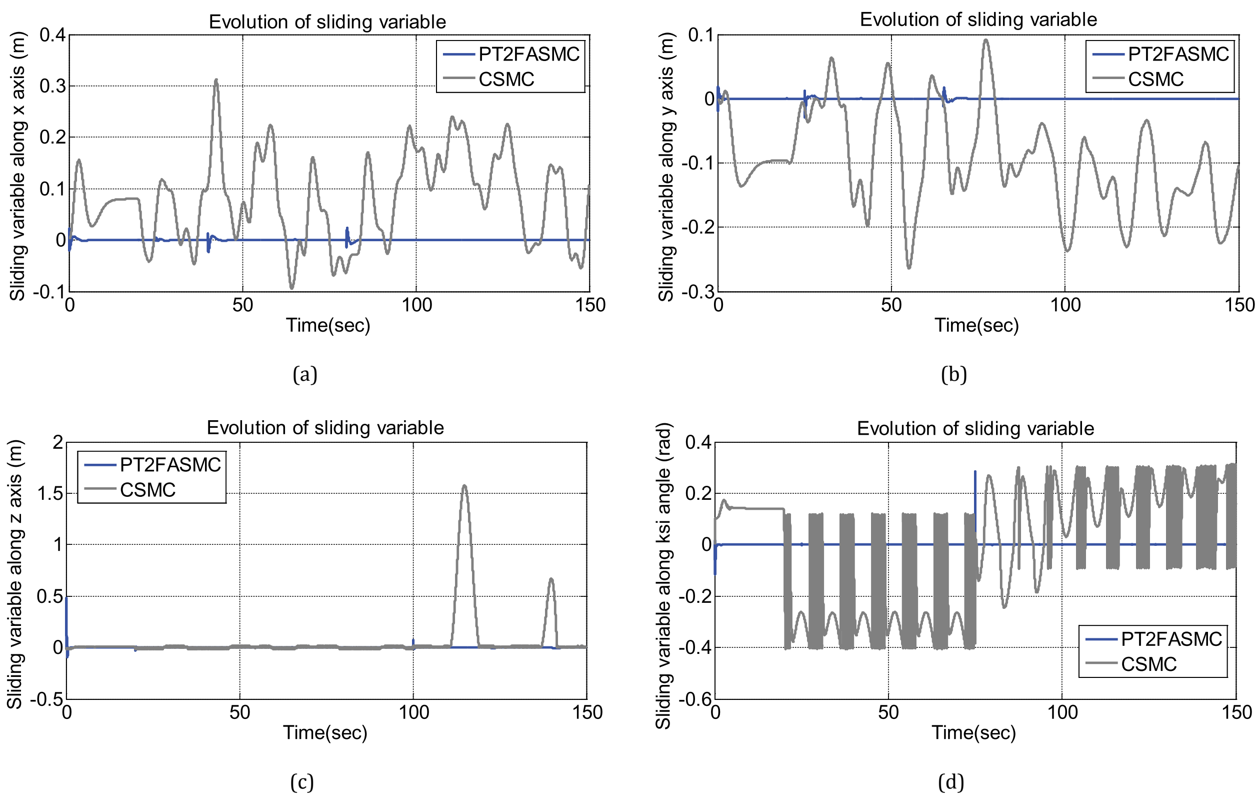

Fig. 14. Sliding surfaces evolution along (x, y, z) axis and yaw angle (ψ) (Scenario 1).

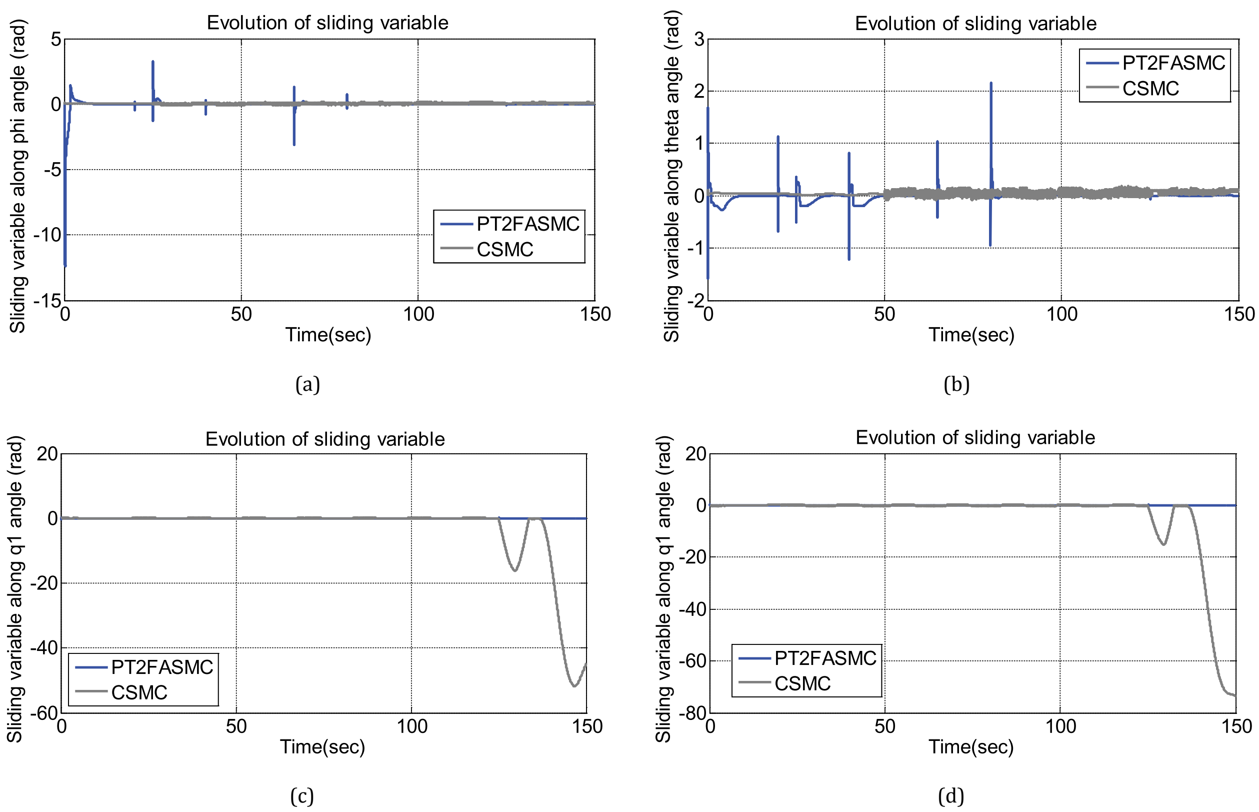

Fig. 15. Sliding surfaces evolution along φ, θ, q_1 and q_2 angles (Scenario 1).

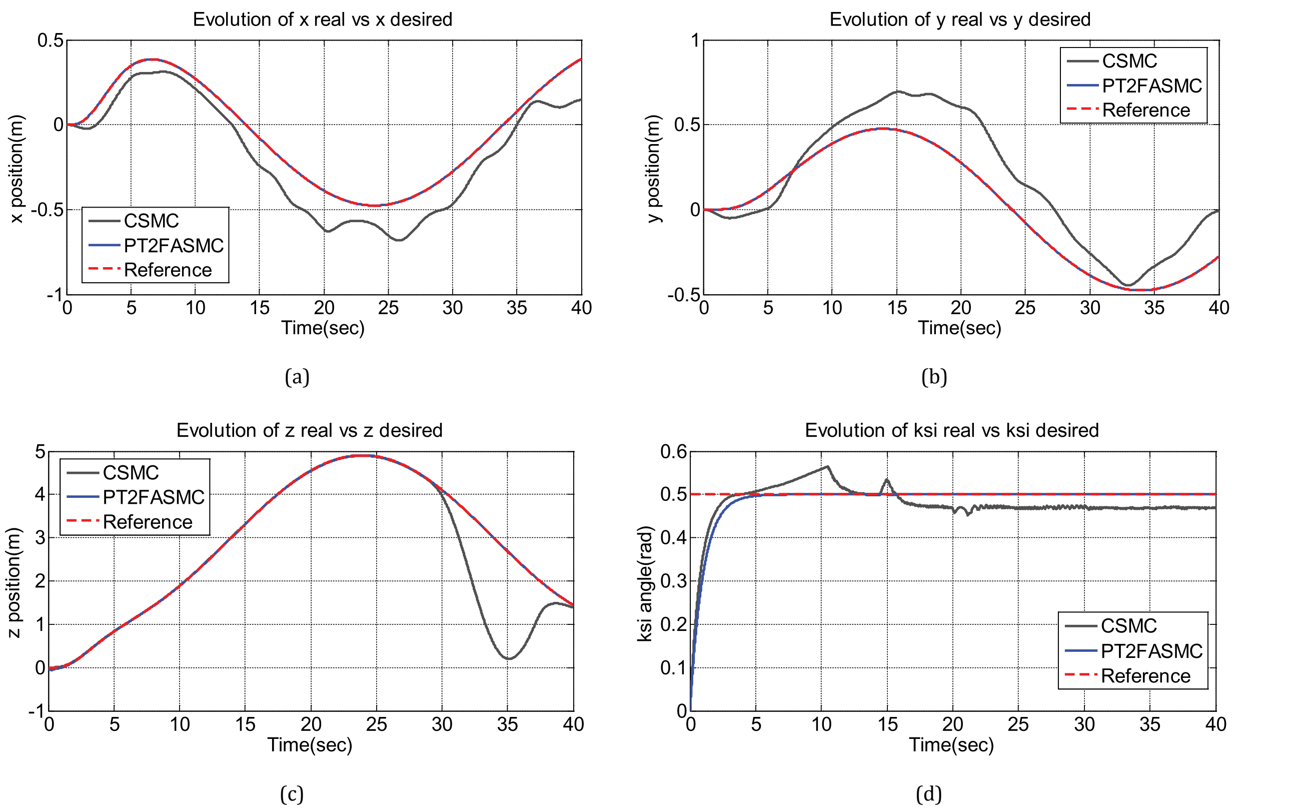

Fig. 16. (x, y, z) positions and yaw angle (ψ) outputs of the UAV in the presence actuator faults, uncertainties and external disturbances (Scenario 2).

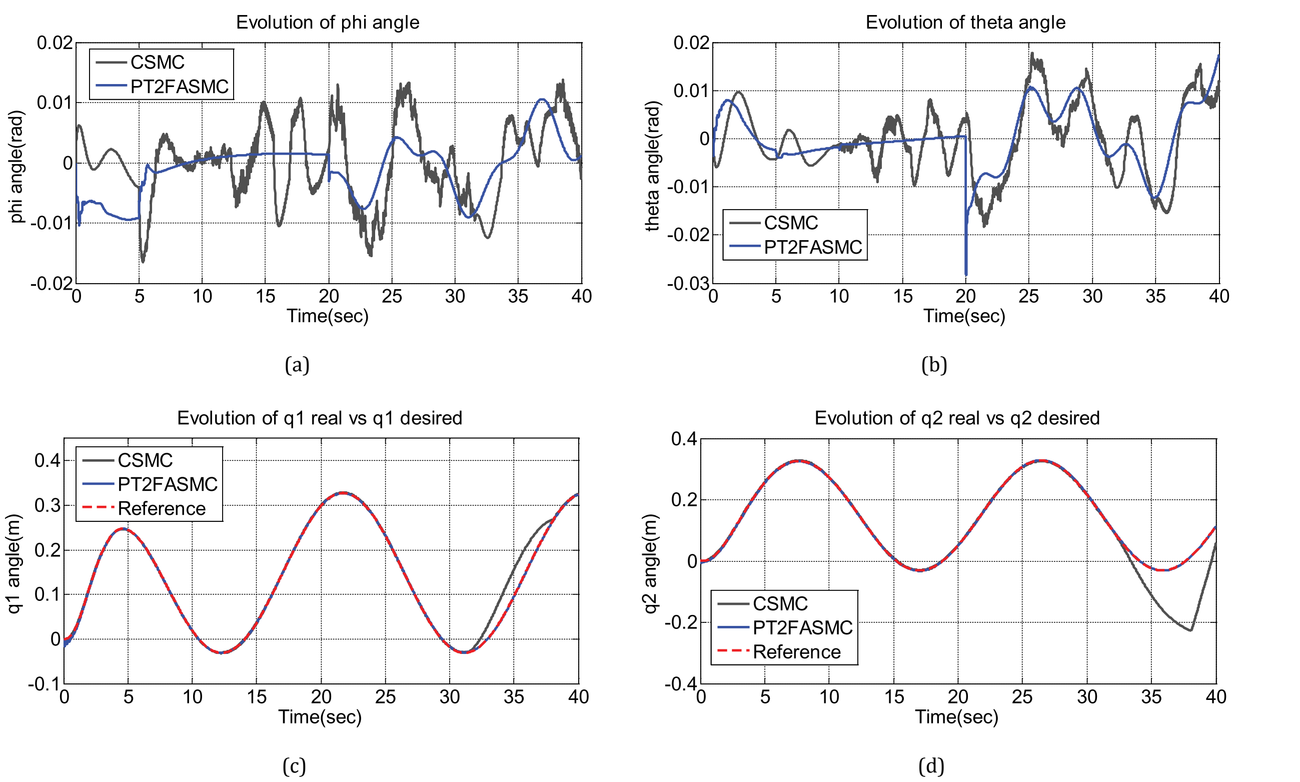

Fig. 17. Roll and pitch angles (φ, θ) of the UAV and q_1 and q_2 angles of the outputs manipulator in the presence actuator faults, uncertainties and external disturbances (Scenario 2).

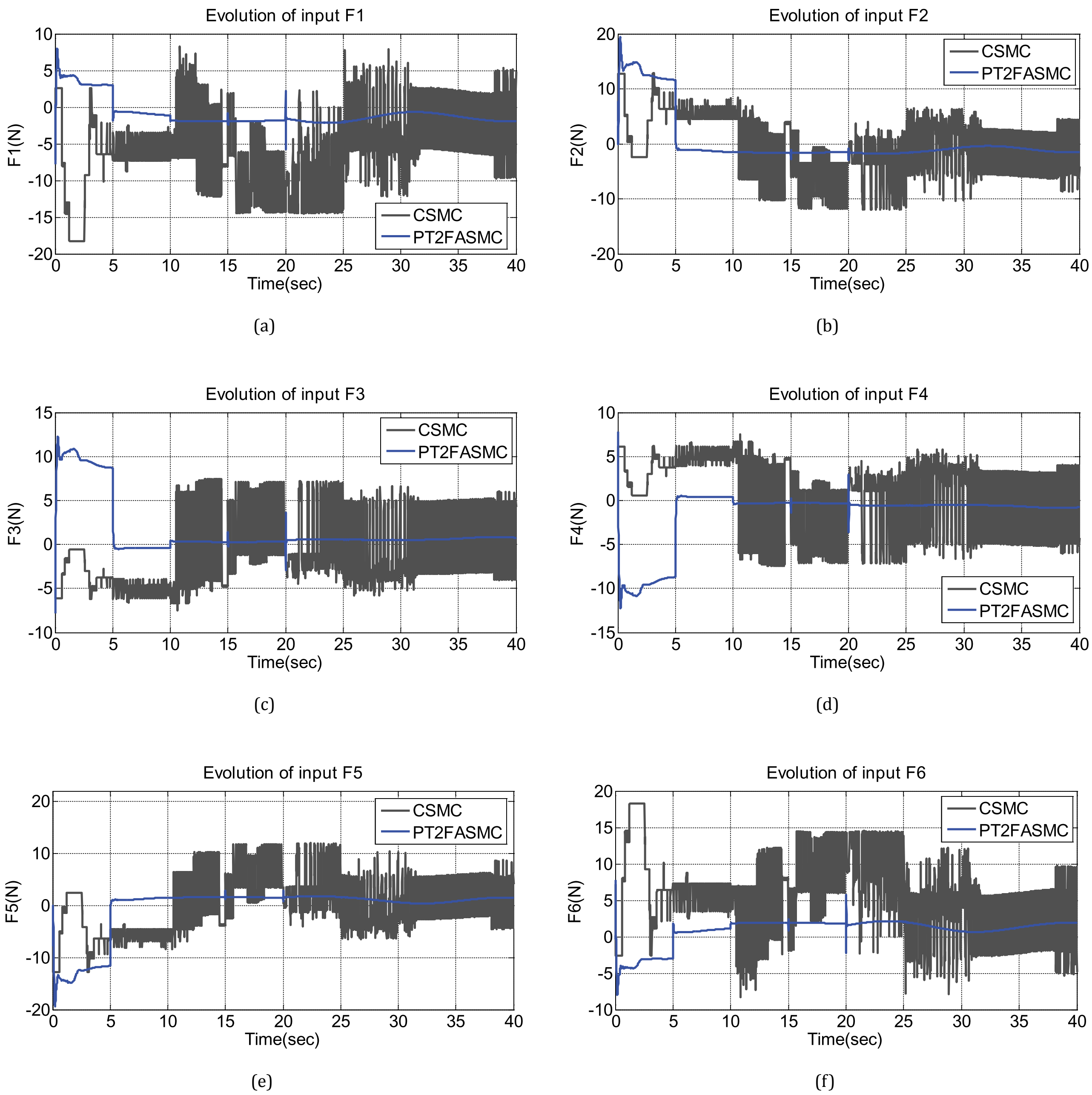

Fig. 18. The six input forces of the UAV (Scenario 2).

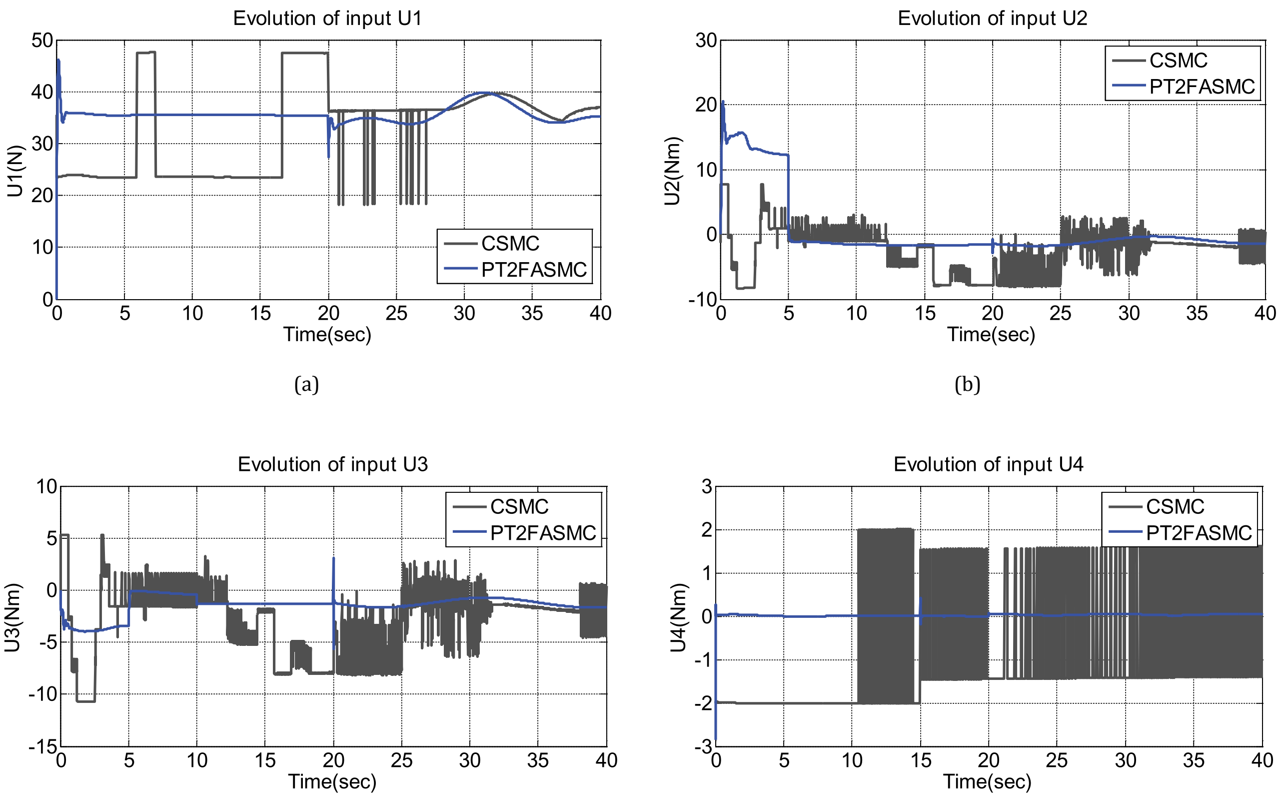

(a) (b)

(c) (d)

Fig. 19. Control inputs of the UAV (Scenario 2).

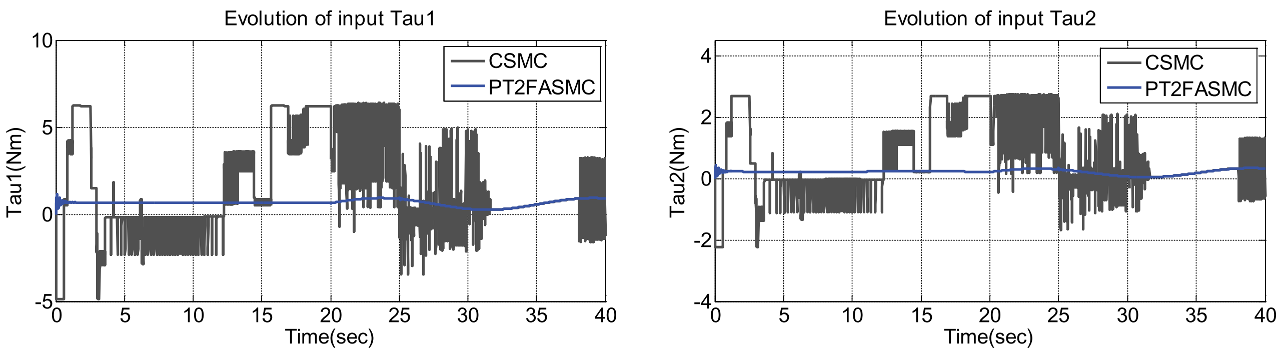

(a) (b)

Fig. 20. Torque control inputs of the manipulator (Scenario 1).

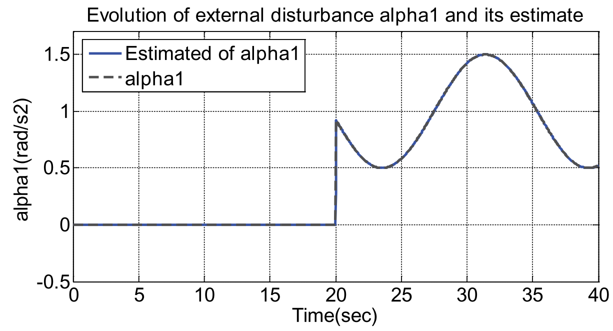

(a)

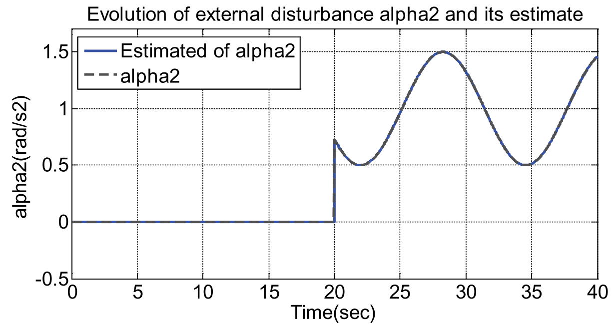

(b)

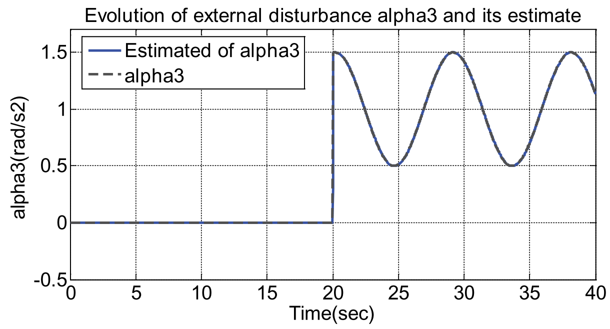

(c)

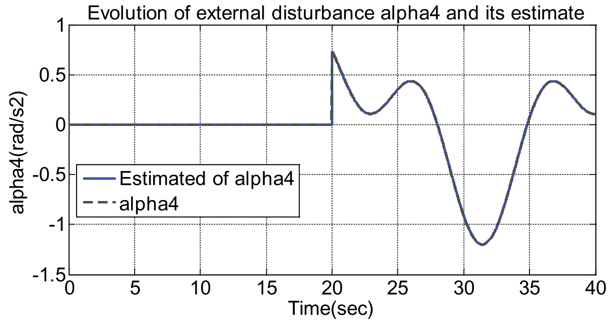

(d)

Fig. 21. α_1, α_2, α_3 and α_4 estimation (Scenario 2).

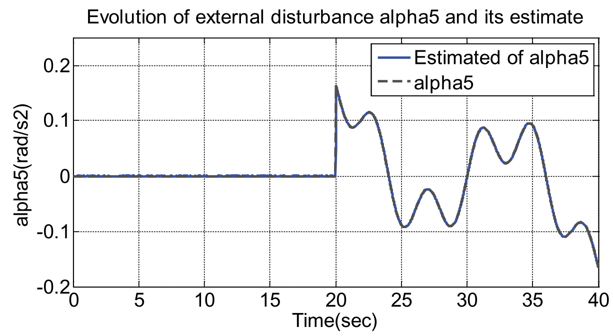

(a)

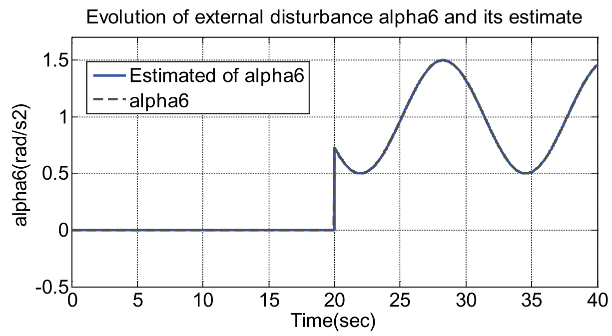

(b)

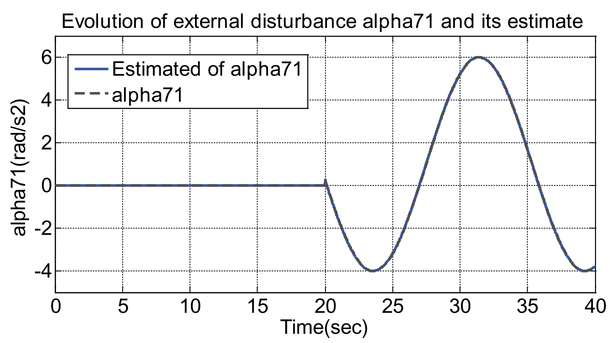

(c)

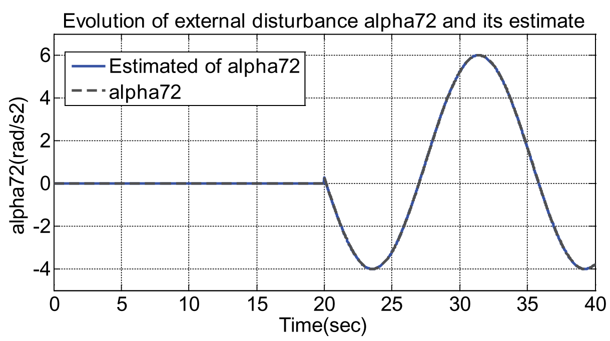

(d)

Fig. 22. α_5, α_6, α_7 and α_8 estimation (Scenario 2).

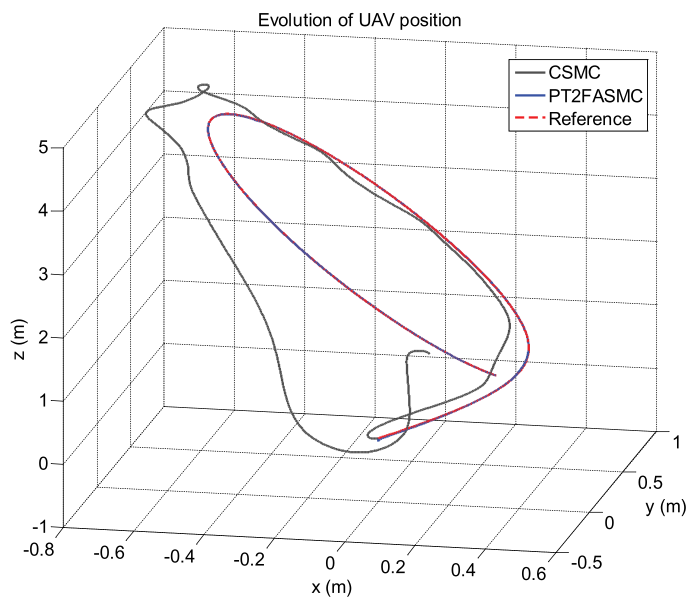

Fig. 23. 3D position tracking result of the UAV.

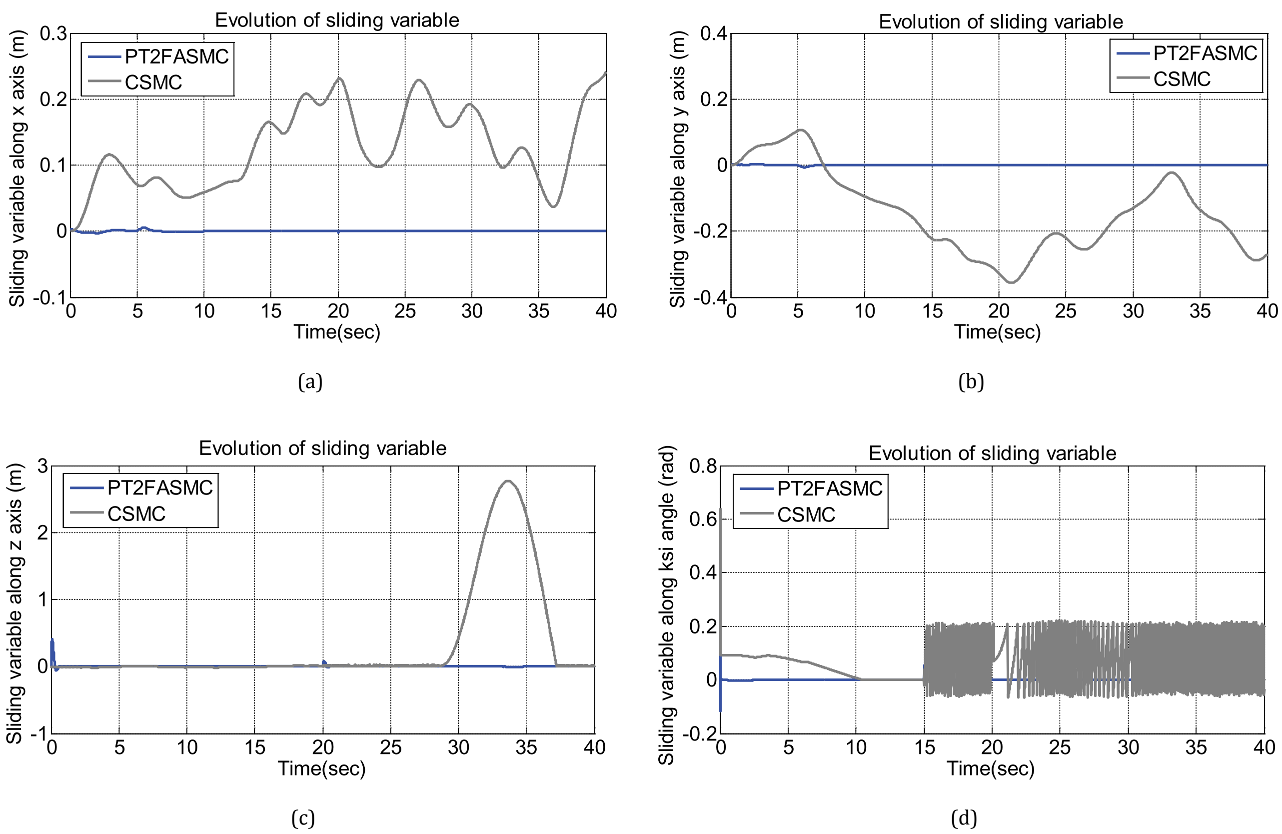

Fig. 24. Sliding surfaces evolution along (x, y, z) axis and yaw angle (ψ) (Scenario 2).

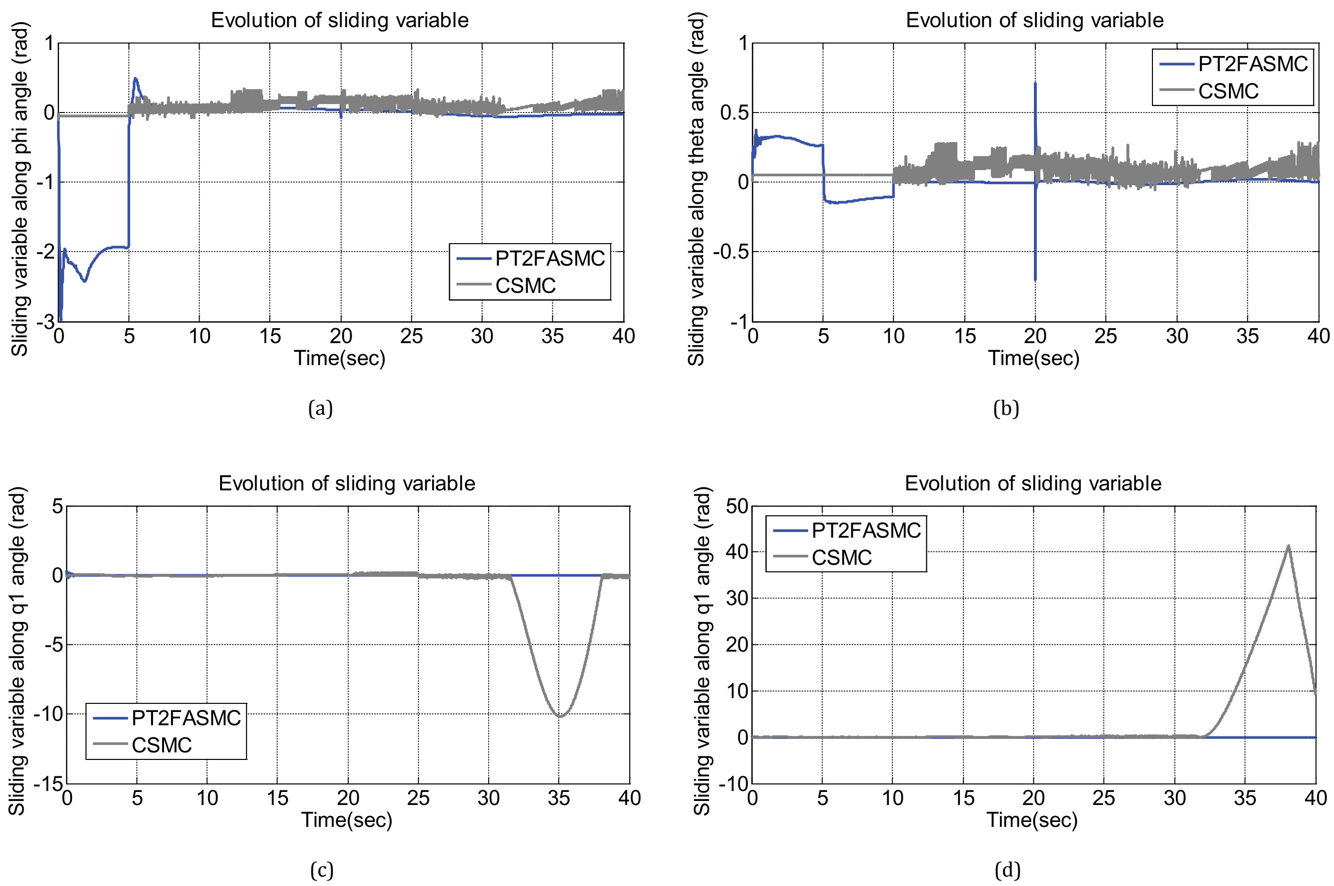

Fig. 25. Sliding surfaces evolution along φ, θ, q_1 and q_2 angles (Scenario 2).

Table 5. Comparison of chattering mitigation between the CSMC and PT2ASMC with $p = 4500$.

Controller	Criterion J_1	Criterion J_2
CSMC	6.13×10^4	5.73×10^4
PT2ASMC	1.03×10^4	2.28×10^4

knowledge of the model of the system to be controlled, which is considered a limitation of this control method.

The disadvantages and limitations of the proposed control approach can be summarized as follows:

- **Complexity:** The disturbance observer-based adaptive type-2 fuzzy fault tolerant control is more difficult than other control systems due to its sophisticated algorithms and design, which require real-time adaptation to dynamic changes.
- **Constraints in fast changes:** In the face of fast system changes, the proposed control approach may need time to adjust, hence impacting performance.
- **Problems involving significant system uncertainties:** While the proposed control algorithm demonstrates robustness, it may encounter challenges in sustaining system performance under conditions of significant system uncertainties.
- **Augmented initial investment:** The sophisticated features of disturbance observer-based adaptive type-2 fuzzy fault-tolerant control result in a generally higher cost than conventional control systems.

8. Performances Comparison With Other Approaches

To make a quantitative comparison between the proposed control method and the controllers proposed in Refs. [45, 46, 55], three well-known performance criteria are used. These are the integral of square error (ISE), integral of the absolute value of the error (IAE) and integral of the time multiplied by the absolute value of the error (ITAE). The obtained values for each criterion are summarized in Table 6 and Fig. 26. It is noted that the proposed control method offers the smallest values control of ISE, IAE and ITAE. In contrast, the proposed control strategy in Refs. [45, 46, 55] presents the largest values of ISE, IAE and ITAE for UAV position (x, y, z). It can be seen that the system performances are better when using the

Table 6. Values of the performance criteria of the proposed control method and the control strategies proposed in Refs. [45, 46, 55] in faulty operation and in the presence of parametric uncertainties and external disturbances.

Control Method	UAV position (x)	UAV position (y)	UAV position (z)
ISE			
Proposed control strategy in [45]	1.37	1.26	1.08
Proposed control strategy in [46]	1.25	1.14	0.95
Proposed control strategy in [55]	1.13	1.05	0.86
Proposed control method	**0.12**	**0.11**	**0.012**
IAE			
Proposed control strategy in [45]	4.63	3.8	0.708
Proposed control strategy in [46]	3.85	2.25	0.910
Proposed control strategy in [55]	3.23	2.05	0.805
Proposed control method	**1.34**	**1.02**	**0.12**
ITAE			
Proposed control strategy in [45]	29.36	22.7	9.38
Proposed control strategy in [46]	25.12	18.5	8.15
Proposed control strategy in [55]	21.32	11.05	6.43
Proposed control method	**10.24**	**7.21**	**1.32**

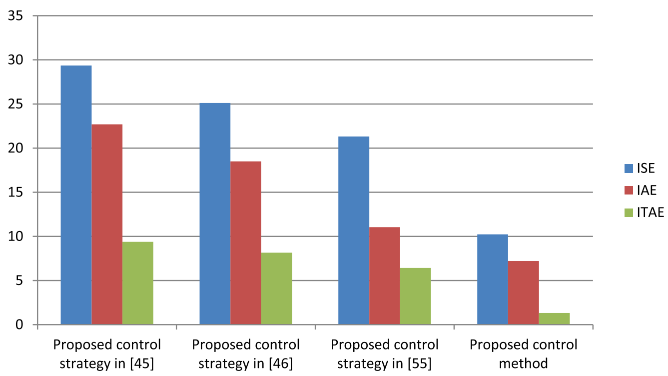

Fig. 26. ISE, IAE and ITAE Histogram of the proposed control algorithm, and the control strategies proposed in Refs. [45, 46, 55].

proposed PT2FASMC as compared to the proposed control strategy in Refs. [45, 46, 55].

9. Conclusion

In this work, an adaptive type-2 fuzzy sliding mode control strategy based on a disturbance observer for MMUAV targets various actuator defects, parametric uncertainties and external disturbances while reducing the chattering phenomenon. Separate processes are employed to overcome actuator faults, parametric uncertainties and external disturbances. Specifically, the suggested adaptive control strategies are used to accommodate parametric uncertainties and actuator faults, while the developed disturbance observer is employed to reduce external disturbances. The discontinuous control strategy of sliding mode control is greatly decreased by using type-2 fuzzy adaptive control parameters in both continuous and discontinuous control sections, preventing chattering phenomena in the control signals. In addition, by combining the suggested disturbance observer with the established adaptive type-2 fuzzy sliding mode control, the discontinuous control gain of sliding mode control is decreased even more. This effectively reduces the chattering phenomena issue while still ensuring the accurate tracking capability of the MMUAV. The control technique described in this study has a much higher level of robustness when compared to earlier research, particularly in dealing with actuator defects, model uncertainties and external disturbances. The efficacy and benefits of the proposed controller are confirmed and justified by numerical simulation tests. These simulations compare the performance of the controller with a conventional sliding mode controller. The MMUAV is subjected to fluctuations in the masses $(m, m_1$ and $m_2)$, varied levels of actuator failures, and unknown external disturbances during these tests.

ORCID

Samir Zeghlache
https://orcid.org/0000-0002-3041-9473
Hilal Rahali
https://orcid.org/0000-0003-1741-3445
Ali Djerioui
https://orcid.org/0000-0001-9597-5975
Loutfi Benyettou
https://orcid.org/0009-0009-6713-0401

Mohamed Fouad Benkhoris
https://orcid.org/0000-0003-0739-7058

References

[1] A.-K. Al-Jioory, Adaptive quadrotor control using online dynamic mode decomposition, *Eur. J. Control* **80**(B) (2024) 101117.

[2] X. Wei, Y. Gan, C. David, S. Carlos, Z. Weidong and H. Wei, Robust collision-free formation control of quadrotor fleets: Trajectory generation and tracking with experimental validation, *Control Eng. Pract.* **145** (2024) 105842.

[3] Ö. Bingöl and H. M. Güzey, Fixed-time neuro-sliding mode controller design for quadrotor UAV transporting a suspended payload, *Eur. J. Control* **73** (2023) 100879.

[4] P. Gasga, F. R. López-Estrada, G. Valencia-Palomo, S. Gómez-Peñate and M. E. Guerrero-Sánchez, Robust convex LPV control of a Helicopter-UAV transporting a suspended payload, *Eur. J. Control* **80**(B) (2024) 101121.

[5] I. Salman, S. Yuhao, A. K. Yasir, K. Maria and J. Umair, Robust adaptive control law design for enhanced stability of agriculture UAV used for pesticide spraying, *Aerosp. Sci. Technol.* **155**(2) (2024) 109676.

[6] S. Hao, C. Guohua, L. Xiaofeng, M. Jinkun, X. Qiming, Z. Lixing and Z. Jie, A novel unmanned aerial vehicle driven real-time situation awareness for fire accidents in chemical tank farms, *J. Loss Prev. Process Ind.* **91** (2024) 105357.

[7] C. Montañez-Molina and J. Pliego-Jiménez, Position and reduced attitude trajectory tracking control of quadrotors: Theory and experiments, *Aerosp. Sci. Technol.* **155**(2) (2024) 109683.

[8] V. N. Lanh, M. K. Ngai and P. H. Quang, Fermat-Weber location particle swarm optimization for cooperative path planning of unmanned aerial vehicles, *Appl. Soft Comput.* **167**(A) (2024) 112269.

[9] Y. L. Ding, B. Xin and J. Chen, A review of recent advances in coordination between unmanned aerial and ground vehicles, *Unmanned Syst.* **9**(2) (2021) 97–117.

[10] J. Wang, A. A. Khalid, B. Yassine, M. Omid and M. Saleh, Adaptive finite-time backstepping control tracker for quadrotor UAV with model uncertainty and external disturbance, *Aerosp. Sci. Technol.* **133** (2023) 108088.

[11] J. E. Julian, N. Endika, M. L. G. Jose and G. Gorka, A low-cost vision system for online reciprocal collision avoidance with UAVs, *Aerosp. Sci. Technol.* **150** (2024) 109190.

[12] N. Algar and J. E. Meng, Command-filtered robust trajectory tracking control for aggressive maneuvers of quadrotor UAV with multiple unknown disturbances, *Eng. Sci. Technol. Int. J.* **59** (2024) 101858.

[13] N. S. Nabarun and K. D. Alok, Dynamic event-triggered neuroadaptive fault-tolerant control of quadrotor UAV with a novel cosine kernel, *Aerosp. Sci. Technol.* **155**(2) (2024) 109643.

[14] M. Mahmood, T. Mostafa, G. G. Pegah and D. Ehsan, Robust fault detection and adaptive fixed-time fault-tolerant control for quadrotor UAVs, *Robot. Auton. Syst.* **179** (2024) 104747.

[15] L. Zuo and L. Yao, Fault isolation and fault tolerant control for the uncertain quadrotor UAV system, *Int. J. Control Autom. Syst.* **22** (2024) 301–310, doi:10.1007/s12555-022-0249-7.

[16] T. Yang, K. Bu, G. Chen, X. Xiangpeng and X. Jianwei, Fault-tolerant multi-rate sampled-data control for quadrotor UAV, *Nonlinear Dyn.* **112** (2024) 12253–12267, doi:10.1007/s11071-024-09691-9.

[17] J. Wang and D. Wang, A robust fault-tolerant control algorithm based on a novel modeling method for quadrotor application with accurate fault estimation, *Evol. Intell.* **17** (2024) 3169–3183, doi:10.1007/s12065-024-00921-y.

[18] S. Mallavalli and A. Fekih, An observer-based backstepping integral nonsingular fast terminal sliding mode fault tolerant control design for quadrotors under different types of actuator faults, *Int. J. Control Autom. Syst.* **21** (2023) 4015–4031, doi:10.1007/s12555-022-0951-5.

[19] T. Li, Y. M. Zhang and B. W. Gordon, Passive and active nonlinear fault-tolerant control of a quadrotor unmanned aerial vehicle based on the sliding mode control technique, *Proc. Inst. Mech. Eng. Part I J. Syst. Control Eng.* **227**(1) (2013) 12–23.

[20] Z. C. Liu, C. Yuan and Y. M. Zhang, Active fault-tolerant control of unmanned quadrotor helicopter using linear parameter varying technique, *J. Intell. Robot. Syst.* **88** (2017) 415–436.

[21] P. Yang, Z. Wang, Z. Zhang and X. Hu, Sliding mode fault tolerant control for a quadrotor with varying load and actuator fault, *Actuators* **10** (2021) 323, doi:10.3390/act10120323.

[22] Y. J. Zhong *et al.*, Active fault-tolerant tracking control of a quadrotorn with model uncertainties and actuator faults, *Front. Inf. Technol. Electron. Eng.* **20**(1) (2019) 95–106.

[23] Y. M. Zhang and J. Jiang, Issues on integration of fault diagnosis and reconfigurable control in active fault-tolerant control systems, *IFAC Proc. Vol.* **39**(13) (2006) 1437–1448.

[24] Z. X. Liu *et al.*, Retrofit fault-tolerant tracking control design of an unmanned quadrotor helicopter considering actuator dynamics, *Int. J. Robust Nonlinear Control* **29**(16) (2019) 5293–5313.

[25] W. Z. Liu *et al.*, Adaptive fault-tolerant formation control for quadrotors with actuator faults, *Asian J. Control* **22**(3) (2020) 1317–1326.

[26] W. Hao and B. Xian, Adaptive fault-tolerant control for a quadrotor UAV based on immersion and invariance methodology, *Nonlinear Dyn.* **90**(4) (2017) 2813–2826.

[27] L. Guo *et al.*, Safety control system technologies for UAVs: Review and prospect, *Sci. Sin. Inform.* **50**(2) (2020) 184–194.

[28] F. Wang *et al.*, Adaptive backstepping sliding mode control of uncertain semi-strict nonlinear systems and application to permanent magnet synchronous motor, *J. Syst. Sci. Complex.* **34**(2) (2021) 552–571.

[29] Y. K. Zhu *et al.*, An enhanced anti-disturbance control law for systems with multiple disturbances, *Sci. China Inf. Sci.* **63**(10) (2020) 209206.

[30] Y. Z. Yang *et al.*, Distributed finite-time integral sliding-mode control for multiagent systems with multiple disturbances based on nonlinear disturbance observers, *J. Syst. Sci. Complex.* **34**(3) (2021) 995–1013.

[31] B. Wang *et al.*, Disturbance observer-based adaptive fault-tolerant control for a quadrotor helicopter subject to parametric uncertainties and external disturbances, *Mech. Syst. Signal Process.* **120** (2019) 727–743.

[32] J. Q. Zhang *et al.*, Robust trajectory tracking controller for quadrotor helicopter based on a novel composite control scheme, *Aerosp. Sci. Technol.* **85** (2019) 199–215.

[33] Y. Y. Wang and J. B. Hu, Robust control for a quadrotor aircraft with small overshoot and high-precision position tracking performance, *J. Franklin Inst.* **357**(18) (2020) 13386–13409.

[34] B. Kang *et al.*, A second-order sliding mode controller of quad-rotor UAV based on PID sliding mode surface with unbalanced load, *J. Syst. Sci. Complex.* **34**(2) (2021) 520–536.

[35] L. X. Xu *et al.*, Backstepping sliding-mode and cascade active disturbance rejection control for a quadrotor UAV, *IEEE/ASME Trans. Mechatronics* **25**(6) (2020) 2743–2753.

[36] K. X. Guo *et al.*, Multiple observers based anti-disturbance control for a quadrotor UAV against payload and wind disturbances, *Control Eng. Pract.* **102** (2020) 104560.

[37] Q. L. Hu, L. Xiao and C. L. Wang, Adaptive fault-tolerant attitude tracking control for spacecraft with time-varying inertia uncertainties, *Chin. J. Aeronaut.* **32**(3) (2019) 674–687.

[38] Y. Y. Guo, B. Jiang and Y. M. Zhang, A novel robust attitude control for quadrotor aircraft subject to actuator faults and wind gusts, *IEEE/CAA J. Autom. Sinica* **5**(1) (2017) 292–300.

[39] S. Zeghlache *et al.*, Fault tolerant control for modified quadrotor via adaptive type-2 fuzzy backstepping subject to actuator faults, *ISA Trans.* **95** (2019) 330–345.

[40] S. Yang, Y. Pan, L. Cao and L. Chen, Predefined-time fault-tolerant consensus tracking control for multi-UAV systems with prescribed performance and attitude constraints, *IEEE Trans. Aerosp. Electron. Syst.* **60**(4) (2024) 4058–4072. doi: 10.1109/TAES.2024.3371406.

[41] X. She, H. Ma, H. Ren and L. Hongyi, Vision-based adaptive prescribed-time control of UAV for uncooperative target tracking with performance constraint, *J. Syst. Sci. Complex.* **37** (2024) 1956–1977, doi:10.1007/s11424-024-3443-2.

[42] A. Kumar and R. K. Shashi, Modified super twisting control for robust trajectory tracking and hovering of quadrotor, *ISA Trans.* **153** (2024) 41–56.

[43] A. Moussa, M. El Mehdi and H. Touria, A new intelligent controller based on integral sliding mode control and extended state observer for nonlinear MIMO drone quadrotor, *Int. J. Intell. Netw.* **5** (2024) 49–62.

[44] I. Mohammadreza and F. Reza, High-gain disturbance observer for robust trajectory tracking of quadrotors, *Control Eng. Pract.* **145** (2024) 105854.

[45] L. Ruobing, Z. Quanmin, N. Hamidreza, Y. Xicai and N. Pritesh, Trajectory tracking of a quadrotor using extend state observer based U-model enhanced double sliding mode control, *J. Franklin Inst.* **360**(4) (2023) 3520–3544.

[46] N. Nguyen and P. Pitakwachara, Integral terminal sliding mode fault tolerant control of quadcopter UAV systems, *Sci. Rep.* **14** (2024) 10786, doi:10.1038/s41598-024-61273-2.

[47] X. Fang, R. Cheng, S. Cheng, C. Songsong and F. Yuan, Nonsingular fixed-time fault-tolerant sliding mode control of robot manipulator with disturbance observer, *Int. J. Control Autom. Syst.* **22** (2024) 2182–2192, doi:10.1007/s12555-022-0594-6.

[48] M. Tianle, A. Halim and E. Christopher, Fault tolerant control of a bio-inspired UAV using sliding mode, *IFAC-PapersOnLine* **58**(4) (2024) 234–239.

[49] K. Ahmed, M. Ibrahim and A. Halim, Fault tolerant control of an octorotor UAV using sliding mode for applications in challenging environments, *Annu. Rev. Control* **57** (2024) 100952.

[50] Q. Huang, E. Zhang, X. Dai, Q. Wu and S. Su, Sliding-mode fault-tolerant control of the six-rotor UAV with dead-zone-input under event-triggered mechanism, *ISA Trans.* **145** (2024) 19–31.

[51] L. Wenxin, X. Pengyang and C. Jian, Disturbance rejection control of the agricultural quadrotor based on adaptive neural network, *Inf. Process. Agric.* (2024), doi:10.1016/j.inpa.2024.05.001.

[52] R. Yong and S. Yaobin, Inverse compensation mechanism-based adaptive fuzzy-neural fault-tolerant control for an uncertain quadrotor UAV, *Aerosp. Sci. Technol.* **153** (2024) 109426.

[53] F. Liao, Z. Zhao and J. Wang, Fault tolerant control of hexarotor UAVs against motor failure, in *Proc. 31st Mediterranean Conf. on Control and Automation* (*MED*), Limassol, Cyprus, 2023, pp. 221–226, doi:10.1109/MED59994.2023.10185903.

[54] H. Liu, Y. Guo, Y. Zhang and J. Bin, Robust fault-tolerant control for quadrotor UAVs with parameter uncertainties and actuator faults, *Control Theory Technol.* **22** (2024) 581–595, doi:10.1007/s11768-024-00228-4.

[55] M. Maaruf, A. N. Abubakar and M. M. Gulzar, Adaptive backstepping and sliding mode control of a quadrotor, *J. Braz. Soc. Mech. Sci. Eng.* **46** (2024) 630, doi:10.1007/s40430-024-05188-z.

[56] O. Salas-Peña, J. DeLeón-Morales and S. V. Gutiérrez-Martínez, Output feedback adaptive super twisting sliding mode control for quadrotor UAVs, *Control Theory Technol.* **22** (2024) 92–105, doi:10.1007/s11768-023-00195-2.

[57] J. Pan, B. Shao, J. Xiong, X. Jiaxin and Z. Qi, Attitude control of quadrotor UAVs based on adaptive sliding mode, *Int. J. Control Autom. Syst.* **21** (2023) 2698–2707, doi:10.1007/s12555-022-0189-2.

[58] Z. Huang, H. Wang and X. Wang, Cascaded fuzzy PID control for quadrotor UAVs based on RBF neural networks, in *Neural Information Processing. ICONIP 2023*, Lecture Notes in Computer Science, Vol. 14447 (Springer, Singapore, 2024), pp. 516–527, doi:10.1007/978-981-99-8079-6_40.

[59] Y. Li, W. Liang and Y. Zheng, Quadrotor aircraft control strategy based on fuzzy PID control, in *Proc. Int. Seminar on Computer Science and Engineering Technology* (*SCSET*), New York, 2023, pp. 648–651, doi: 10.1109/SCSET58950.2023.00147.

[60] X. Wenhao, Q. Qingjie, L. Wengang, L. Yingjie, L. Dan and W. Yue, Control of quadrotor robot via optimized nonlinear type-2 fuzzy fractional PID with fractional filter: Theory and experiment, *Aerosp. Sci. Technol.* **151** (2024) 109286.

[61] J. D. Bošković and R. K. Mehra, Failure detection, identification and reconfiguration in flight control, in *Fault Diagnosis and Fault Tolerance for Mechatronic Systems: Recent Advances* (Springer, Berlin, 2003), pp. 127–167.

[62] O. Rodríguez-Abreo, F. J. Ornelas-Rodríguez, A. Ramírez-Pedraza, J. B. Hurtado-Ramos and J. J. González-Barbosa, Backstepping control for a UAV-manipulator tuned by Cuckoo Search algorithm, *Robot. Auton. Syst.* **147** (2022) 103910.

[63] T. Madani and A. Benallegue, Sliding mode observer and backstepping control for a quadrotor unmanned aerial vehicles, in *Proc. 2007 American Control Conf.*, New York, 2007, pp. 5887–5892, doi: 10.1109/ACC.2007.4282548.

[64] F. Wang, Z. Ma, H. Gao and H. Changchun, Disturbance observer-based nonsingular fast terminal sliding mode fault tolerant control of a quadrotor UAV with external disturbances and actuator faults, *Int. J. Control Autom. Syst.* **20** (2022) 1122–1130.

[65] B. Wang, Y. Zhang and W. Zhang, A composite adaptive fault-tolerant attitude control for a quadrotor UAV with multiple uncertainties, *J. Syst. Sci. Complex.* **35** (2022) 81–104, doi:10.1007/s11424-022-1030-y.

[66] Q. Liang and J. M. Mendel, An introduction to type-2 TSK fuzzy logic systems, in *Proc. IEEE Int. Fuzzy Systems Conf.*, Seoul, Korea, 1999, pp. 1534–1539.

[67] N. N. Karnik, J. M. Mendel and Q. Liang, Type-2 fuzzy logic systems, *IEEE Trans. Fuzzy Syst.* **7**(6) (1999) 643–658.

[68] W.-H. Chen, J. Yang, L. Guo and S. Li, Disturbance-observer-based control and related methods–an overview, *IEEE Trans. Ind. Electron.* **63**(2) (2016) 1083–1095.

[69] B. Xian, S. Z. Wang and S. Yang, Nonlinear adaptive control for an unmanned aerial payload transportation system: Theory and experimental validation, *Nonlinear Dyn.* **98**(3) (2019) 1745–1760.

[70] A. Benaddy, M. Labbadi and M. Bouzi, Robust flight control for a quadrotor under external disturbances based on generic second order sliding mode control, *IFAC-PapersOnLine* **55**(12) (2022) 270–275.

Samir Zeghlache was born in Setif, Algeria, in 1984. He received the Engineer degree in Electrical Engineering from the University of M'Sila (Algeria) in June 2006 and the Magister degree in electrical engineering from Military Polytechnic School of Algiers (Algeria) in January 2009. He received the Ph.D. degree in Electronics from M'Sila University (Algeria), in 2014. Since 2011, he has held a teaching and research position in the Department of Electrical Engineering of M'sila University (Algeria), and he is still part of lecturing staff as Associate Professor. His current research interests include nonlinear system control.

Hilal Rahali was born in M'sila, Algeria, in 1983 received his Engineer degree and Magister degree in Electrical engineering from National Polytechnic School in Algiers, Algeria, in 2008 and 2011, respectively, and he received his Ph.D degree in Electrical Engineering from the University of M'sila, Algeria in 2020. He is currently working as a professor Lecturer and researcher in Electrical Engineering department, Faculty of Technology at University of M'sila, Algeria. His current research interests electrical machines and drives modeling and analysis, nonlinear control, Fault tolerant control of electrical machines.

Ali Djerioui was born in M'sila, Algeria, in 1986. He received the Engineering degree in electrical engineering from the University of Mohamed Boudiaf, M'sila, Algeria, in 2009, the M.Sc. degree in electrical engineering from Polytechnic Military Academy, Algiers, Algeria, in 2011, the doctorate degree in electronic instrumentation systems from the University of Science and Technology Houari Boumediene, Bab Ezzouar, Algeria, in 2016, and the "HDR" degree in electrical engineering, in May 2018. He is currently an Assistant Professor with the University of Mohamed Boudiaf. His current research interests include power electronics, control, microgrids, and power quality.

Loutfi Benyettou was born in M'sila, Algeriain 1979. He received his Engineer degree in Electronics and Magister degree in industrial control from M'sila University in 2002 and 2006 respectively. He received his Ph.D. in electrical engineering from Bechar University (Algeria), in 2016. Currently, he is an Professor in the Department of Electrical Engineering of M'sila University. His scientific interests are power quality conditioning, DSP and digital control, control and diagnostic. He is member of several research projects at University of M'sila and Electrical Engineering Laboratory of M'sila University.

Mohamed Fouad Benkhoris was born in Bou-sâada, Algeria, on September 17, 1963. He received the Engineering degree from the Ecole Nationale Polytechnique d'Alger, El Harrach, Algeria, in 1986, the Ph.D. degree from the l'Institut National Polytechnique de Lorraine, Nancy, France, in 1991, and the HDR degree, in March 2004, all in electrical engineering. Since 2006, he has been a Professor with Polytech-Nantes, Nantes, France. He is currently the Deputy Director of Polytech Nantes. He makes research activities at the laboratory IREENA Saint Nazaire. His fields of interest are control of electrical drives and especially multiphase drive, multiconverters systems embarked network, and renewable energy.